

**REPORT DOCUMENTATION PAGE**

Form Approved OMB No. 0704-0188

Public reporting burden for this collection of information is estimated to average 1 hour per response, including the time for reviewing instructions, searching existing data sources, gathering and maintaining the data needed, and completing and reviewing the collection of information. Send comments regarding this burden estimate or any other aspect of this collection of information, including suggestions for reducing the burden, to Department of Defense, Washington Headquarters Services, Directorate for Information Operations and Reports (0704-0188), 1215 Jefferson Davis Highway, Suite 1204, Arlington, VA 22202-4302. Respondents should be aware that notwithstanding any other provision of law, no person shall be subject to any penalty for failing to comply with a collection of information if it does not display a currently valid OMB control number.  
**PLEASE DO NOT RETURN YOUR FORM TO THE ABOVE ADDRESS.**

<b>1. REPORT DATE (DD-MM-YYYY)</b> 26-07-2010	<b>2. REPORT TYPE</b> Final Report	<b>3. DATES COVERED (From – To)</b> 23 July 2009 - 23-Jul-10
--	---------------------------------------	---

<b>4. TITLE AND SUBTITLE</b>  Discharge atomic iodine generator (DAIG) for a COIL	<b>5a. CONTRACT NUMBER</b> FA8655-09-1-3092
	<b>5b. GRANT NUMBER</b>
	<b>5c. PROGRAM ELEMENT NUMBER</b>

<b>6. AUTHOR(S)</b>  Dr. Jarmila Kodymová	<b>5d. PROJECT NUMBER</b>
	<b>5d. TASK NUMBER</b>
	<b>5e. WORK UNIT NUMBER</b>

<b>7. PERFORMING ORGANIZATION NAME(S) AND ADDRESS(ES)</b> Institute of Physics, Academy of Sciences CR Na Slovance 2 Prague 8 182 21 Czech Republic	<b>8. PERFORMING ORGANIZATION REPORT NUMBER</b>  N/A
---	--

<b>9. SPONSORING/MONITORING AGENCY NAME(S) AND ADDRESS(ES)</b>  EOARD Unit 4515 BOX 14 APO AE 09421	<b>10. SPONSOR/MONITOR'S ACRONYM(S)</b>
	<b>11. SPONSOR/MONITOR'S REPORT NUMBER(S)</b> Grant 09-3092

**12. DISTRIBUTION/AVAILABILITY STATEMENT**  
Approved for public release; distribution is unlimited.

**13. SUPPLEMENTARY NOTES**

**14. ABSTRACT**

This report results from a contract tasking Institute of Physics, Academy of Sciences CR as follows: B.Technical Proposal / Description of Work:  
 The results and experience gathered during the previous contract can be a good base for the following-on research on this subject. We would like to solve the remaining problems and improve this alternative method of atomic iodine generation. The work on these tasks can be described as follows:  
 To increase the efficiency of atomic iodine generation, i.e. a dissociation degree and atomic iodine number density with CH3I and CF3I by:  
 (i) optimization of experimental conditions by adding small amounts N2 or NO into the gas discharge mixture,  
 (ii) optimization of plasma conditions by RF power loaded into the discharge chamber, shortening the wolfram rod electrode, and a more delicate impedance matching,  
 (iii) by other configuration of injector holes to decrease the cavity pressure;

**15. SUBJECT TERMS**  
EOARD, Laser modeling, Chemical oxygen iodine lasers, Laser engineering

<b>16. SECURITY CLASSIFICATION OF:</b>			<b>17. LIMITATION OF ABSTRACT</b> UL	<b>18, NUMBER OF PAGES</b>  40	<b>19a. NAME OF RESPONSIBLE PERSON</b> A. GAVRIELIDES
<b>a. REPORT</b> UNCLAS	<b>b. ABSTRACT</b> UNCLAS	<b>c. THIS PAGE</b> UNCLAS			<b>19b. TELEPHONE NUMBER</b> (Include area code) +44 (0)1895 616205

DEPARTMENT OF THE AIR FORCE  
HEADQUARTES, 603D REGIONAL SUPPORT GROUP (USAFE)  
**European Office of Aerospace Research and Development (EOARD)**

---

# Final Report

Referring to

**Grant # FA8655-09-1-3092**

**Performance 23 July 2009 – 22 July 2010**

**Title:** Discharge Atomic Iodine Generator (DAIG) for a COIL

**Principal Investigator** Jarmila Kodymová

**Co-Investigators** Vít Jirásek, Josef Schmiedberger, Miroslav Čenský

**Grant Awarded to** Institute of Physics, Academy of Sciences CR  
Na Slovance 2  
182 21 Prague 8  
Czech Republic  
Phone: +420 266 052 699  
Fax: +420 286 890 265  
E-mail: [kodym@fzu.cz](mailto:kodym@fzu.cz)

**Technical Advisor** Dr. Timothy Madden  
High Power Gas Lasers Branch  
USAF Research Laboratory Directed Energy Directorate  
Kirtland AFB, NM, USA

**Date of Submission** 22 July 2010, i.e. 12 months after start of period of performance

## Contents

1. General outline of the grant.....	3
1.1. Outline of the grant subject and motivation.....	3
1.2. Main achievements during the previous EOARD grant.....	3
1.3. Tasks and supplies of this grant proposal.....	3
2. Description of the DAIG device .....	4
3. Design and manufacturing of modified iodine injectors.....	7
4. Design and manufacturing of new solid I <sub>2</sub> evaporator.....	9
4.1. Evaporator hardware.....	9
4.2. Operation of I <sub>2</sub> evaporation system.....	12
5. Theoretical background for evaluation of experimental results.....	14
6. Results of investigation of several atomic iodine donors.....	15
6.1. Investigation of alkyl iodides CH <sub>3</sub> I and CF <sub>3</sub> I dissociation.....	15
6.1.1. Measurements in CW RF discharge; injector with circular injection holes used.....	15
6.1.2. Measurements in CW RF discharge; injector with oval injecting holes used.....	20
6.1.3. Measurements in repetitively pulsed RF discharge.....	24
6.1.4. Post-discharge modeling of recombination.....	25
6.2. Investigation of HI dissociation.....	27
6.3. Investigation of I <sub>2</sub> dissociation.....	29
6.4. Comparison of four iodine donors studied in DAIG.....	36
7. Conclusions.....	37
8. References.....	38
Acknowledgements.....	40

## **1. General outline of the grant**

### **1.1. Outline of the grant subject and motivation**

The grant is a continuation of the EOARD Grant No. FA8655-06-1-3034 “Discharge generation of atomic iodine for a COIL” that was finished by submitting the Final EOARD report on 15 May 2008, and was aimed at development of an alternative method of the atomic iodine generation for a COIL by a discharge plasma decomposition of iodine compounds. Motivation of this research followed from some disadvantages of the conventional method using solid or liquid I<sub>2</sub> vapour decomposition to iodine atoms by energy of singlet oxygen: a loss of O<sub>2</sub>(<sup>1</sup>Δ) energy in the dissociation process (by theoretical estimation 4–10 O<sub>2</sub>(<sup>1</sup>Δ) / I<sub>2</sub>), unfavorable kinetic problem of the fast quenching of I\* ( $k = 3.1 \times 10^{-11} \text{ cm}^3 \text{ molec}^{-1} \text{ s}^{-1}$ ) by a superfluous I<sub>2</sub> in the laser medium, and also a problematic controlling the I<sub>2</sub> flow rate into a mixing region of the laser. The research has been performed on originally designed and constructed Discharge Atomic Iodine Generator (abr. DAIG).

### **1.2. Main achievements during the previous EOARD grant No. FA8655-06-1-3034**

Construction of the whole DAIG device was completed, including all needed measuring and diagnostic instruments; special software for experimental data acquisition under the LabView (National Instruments, USA) was developed.

A comprehensive literature review of physical properties of iodine donor compounds potentially considered for experimental investigation in framework of the grant was made.

Two alkyl iodides, CH<sub>3</sub>I and CF<sub>3</sub>I were chosen for the initial research on the discharge dissociation and atomic iodine generation. The number density of iodine atoms was up to  $1 \times 10^{15} \text{ cm}^{-3}$  in the subsonic flow, and did not exceed  $1.4 \times 10^{14}$  in the supersonic flow. The RI dissociation fraction was up to 17% with CH<sub>3</sub>I and up to 21% with CF<sub>3</sub>I. The experimental conditions were not optimized yet.

The detailed results of this research were described in the Interim Reports and Final Report of this grant [1] and in publications [2-6].

### **1.3. Tasks and supplies of this grant proposal**

- Increase in the efficiency of atomic iodine generation from CH<sub>3</sub>I and CF<sub>3</sub>I, i.e. increase in the dissociation degree and atomic iodine number density. This should be achieved by:
  - (i) optimization of gas flow conditions and adding small amounts of N<sub>2</sub> or NO into the gas

discharge mixture; (ii) optimization of plasma conditions (e.g., increase in the RF power loaded into the discharge chamber, shortening the RF rod electrode, etc.), (iii) a new configuration of the iodine injector holes to decrease pressure in the RF chamber;

- Testing a pulse-periodic RF discharge, which should result in gas temperature decrease and influence the discharge kinetics;
- Research extending to other iodine donor molecules, e.g. HI and I<sub>2</sub>, and comparing of the atomic iodine yield and other generation parameters for all iodine donors;
- Testing the DAIG device with the primary flow containing O<sub>2</sub>(<sup>1</sup>Δ) by joining it to either chemical or discharge singlet oxygen generator; small signal gain measurement;
- Detection of the emission spectra of the discharge and afterglow using the Advantest analyzer; special attention paid to presence of I<sup>\*</sup>;
- Support of experimental work by the numerical modeling; study of recombination and quenching processes by e.g. R• radicals, R-R dimmers, etc.  
(*next year of the contract – Option*);
- Study of other iodine donor molecules, e.g., CHI<sub>3</sub>, C<sub>3</sub>F<sub>7</sub>I  
(*next year of the contract – Option*);

## 2. Description of the DAIG device

The DAIG device operates on principle of dissociation of suitable iodine-containing compounds, e.g. alkyl iodides CH<sub>3</sub>I, CF<sub>3</sub>I or HI, I<sub>2</sub>, by means of the RF discharge. Principle of the device configuration is schematically shown in **Fig. 1**. A cylindrical discharge chamber with tungsten rod electrode located coaxially forms simultaneously the iodine injector. This key component of the DAIG device has a special shape forming with the cavity walls a double slit nozzle for choking the primary gas flow. It was designed by the 2-D method of characteristics, 1-D isentropic flow calculations and CFD modeling. The Mach number 2 was presupposed in the expansion region for the primary gas flow composed of O<sub>2</sub>/He mixture (1:2, κ = 1.547). The calculations counted with the expansion ratio  $A_{\text{exp}} / A_{\text{throat}} = 2.5$ , the nozzle throat width 50 mm, and a vacuum pumping system of the nominal capacity  $Q = 3000 \text{ m}^3/\text{h}$ . A technical drawing of this device element is in **Fig. 2**, and the most important parts of the device are shown also in **Fig. 3**.

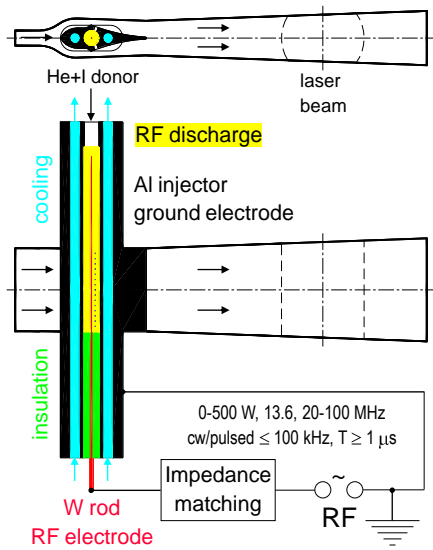


**Fig. 1.** DAIG principle

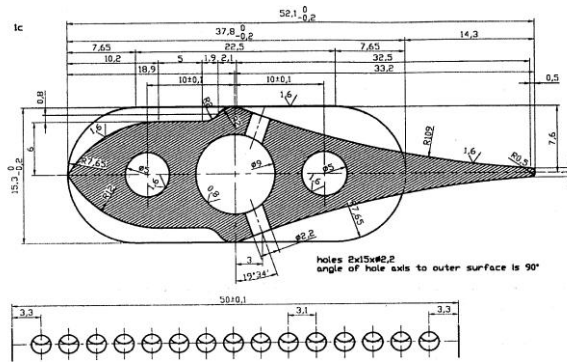


**Fig. 2.** RF discharge cavity (middle hole) and cooling channels inside the atomic iodine injector, forming a double-slit nozzle

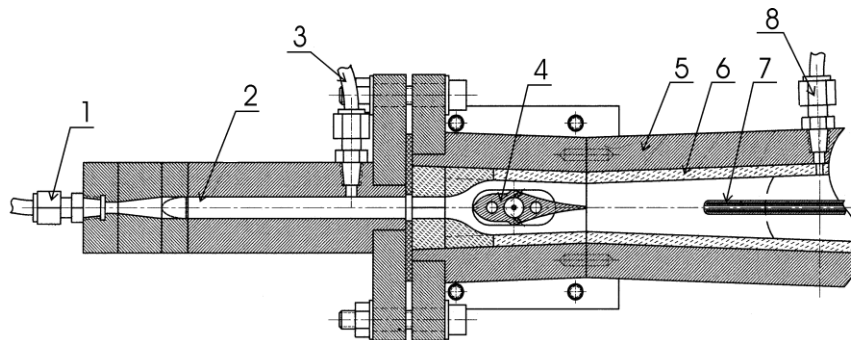


**Fig. 3.** Side view of DAIG device cross section

- 1 – inlet of primary gas flow; 2 – subsonic duct; 3 – pressure detection in subsonic duct;
- 4 – unit of discharge cavity/ iodine injector/double slit nozzle; 5 – Plexiglas supersonic cavity;
- 6 – sheet glass; 7 – Pitot tube; 8 – pressure detection

The injector was made of pure aluminum (99.5% Al, A1050). A middle channel of 9 mm i.d. forms the discharge chamber with axially inserted RF tungsten electrode of 2 mm o.d. The electrode is directly connected to the RF impedance matching box. The left and right channels in Fig. 2 of inner diameter 5 mm are used for cooling the discharge chamber by water. The injector orifices in Fig. 2 were designed by means of correlations of a non-dimensional penetration parameter and 3-D modeling of the atomic iodine mixing in the supersonic cavity.

The whole DAIG device and measuring technique with the Iodine Scan diagnostics can be seen on **Photo 1** from the front view (without the gas handling and their flow controlling, iodine trap, vacuum system).

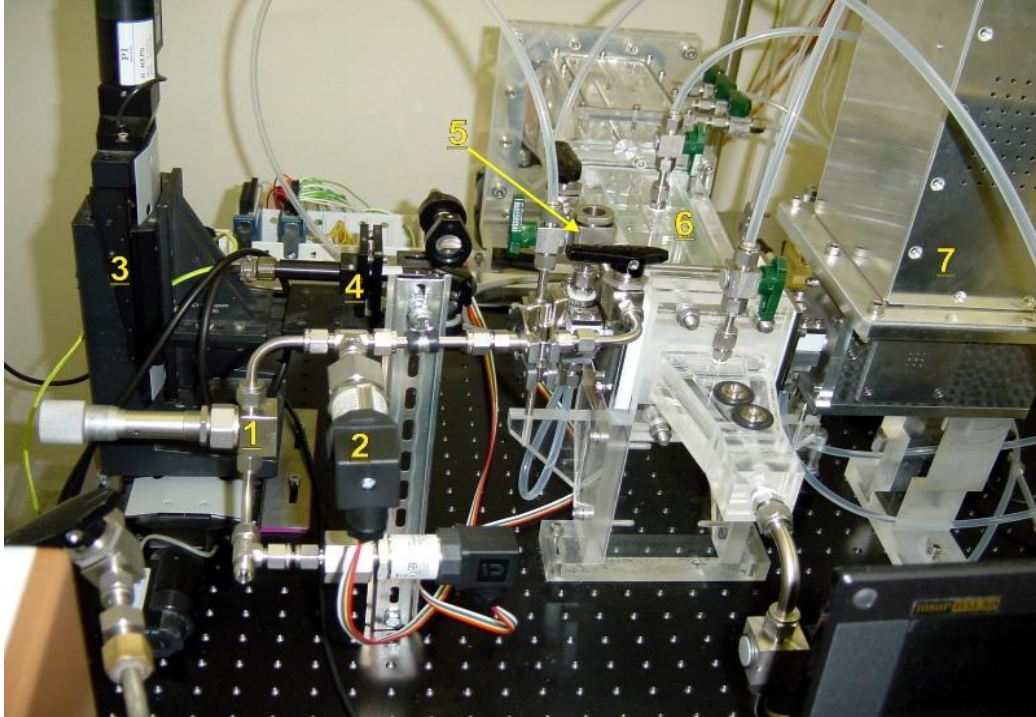


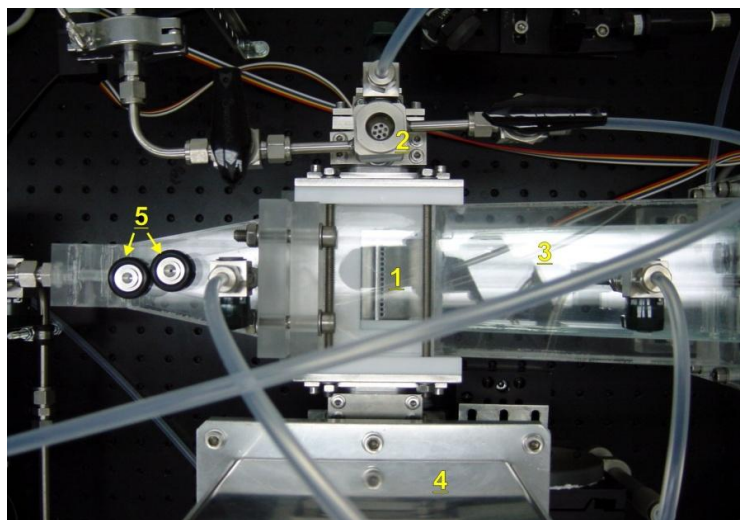
**Photo 2.** View on the whole device and measuring techniques

- 1 – needle valve for adjusting of iodine donor flow rate, 2 – pressure gauge, 3 – moving stage for ISD diagnostics, 4 – ISD probe, 5 – mixing chamber for inlet of iodine donor and carrier gas, 6 – region for atomic iodine detection (supersonic cavity), 7 – impedance matching box

A mixing chamber (**Photo 2 - 2**) for a fast vortex mixing of iodine donor ( $\text{CH}_3\text{I}$  or  $\text{CF}_3\text{I}$ ) and carrier gases (mixture of Ar and He) was designed as a small stainless steel cylindrical vessel of inner volume of  $\sim 1.1 \text{ cm}^3$  with three gas ports and one window.

**Photo 2.** Device details

- 1 – injector/double slit nozzle, 2 – mixing chamber of iodine donor with carrier gas, 3 – supersonic cavity, 4 – RF impedance matching box, 5 – diaphragms for flow rate measurement



Gas flow rates were measured by means of originally proposed flow meters based on the measurement of the pressure upstream and downstream the needle valve or, in case of alkyl iodides, sonic orifices. Both types were calibrated by means of mass flow meters. Pressure in several important points of the DAIG device was measured by electric pressure transducers of strain gauge type. The USB Data Acquisition System (National Instruments Comp., USA) was used to record signals from all pressure transducers, and data were processed by PC on-line under the LabView software. The RF power source (Pearl Kogyo Co., Ltd., Japan) was a wideband tunable cw/pulse radiofrequency generator with oscillation frequency 20-100 MHz, output power  $\leq 500$  W, and a possible pulse-periodic mode with frequency of 100 Hz – 99 kHz, using the pulse duty 5-95 %.

The PSI Iodine Scan Diagnostics (further ISD) based on a narrow band tunable diode probe laser was used for evaluation of atomic iodine concentrations and temperature in the cavity by measuring absorption for the  $I(^2P_{1/2}) - I(^2P_{3/2})$  transition at 1315 nm. The ISD probe beam emitter/detector unit was mounted on the assembly of motorized linear positioning equipment controlled by PC.

A detailed description of the device and diameters of individual parts can be found in the EOARD Report of the previous grant [1], and the Interim report of this grant [7].

### **3. Design and manufacturing of modified iodine injectors**

Within the research period of this grant, modeling results of pressure conditions in the discharge chamber revealed that better dissociation of iodide RI and reducing the wall iodine atoms recombination during the passage through the injector holes would be attained at a decreased pressure in the discharge chamber. This was not however achievable with the previously used injector configuration having circular holes because their diameter could not be increased for a geometrical reason. This problem was therefore solved by increase in the cross-section of the holes in direction of the primary flow. A drawing of the new injector is shown in **Fig. 4**. Fifteen holes are in two opposite rows, a shorter diameter of each hole is 2 mm, and a longer diameter is 3.3 mm, which means that the former cross-section of all injector holes was multiplied by a factor of 1.5.

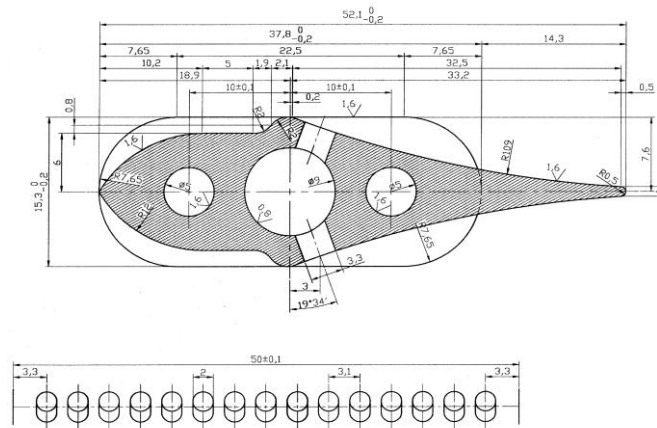


**Fig. 4.** Technical drawing of the supersonic injector with oval holes

To judge a mixing function of the new injector, a CFD modeling was performed to simulate mixing of primary and secondary flows using  $N_{2,prim}$  and  $Ar_{sec}$ . The maximum Mach number of 1.97 was calculated, and mixing of the injected Ar with  $N_2$  primary flow was satisfactory – see **Fig. 5**.

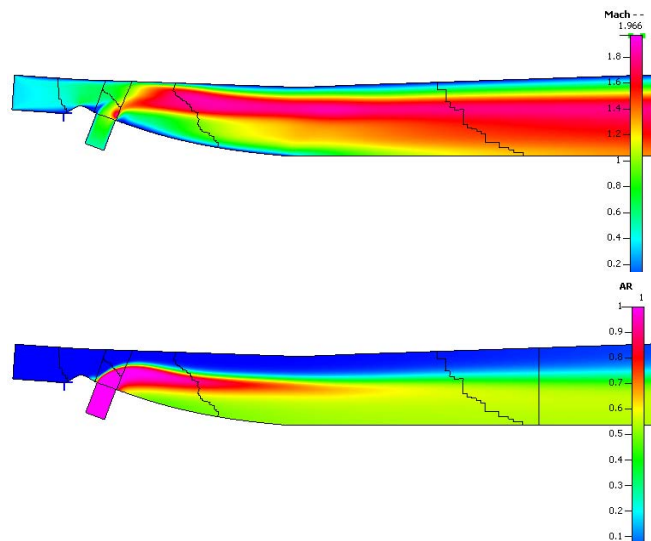


**Fig. 5.** Contours of Mach number and Ar mass fraction for the injector with oval holes  
 Calculated for 20 mmol/s  $N_2$ , 9.63 mmol/s Ar; pressure at holes inlet 1126 Pa

To improve an effective expansion of relatively low flow rates of monatomic gases (He, Ar) to a supersonic velocity, the cross-section of the supersonic nozzle throat formed by the space between the injector and the cavity walls (2 times 4 x 50 mm) should be decreased. One possibility how to solve this problem would be a transonic injection. We therefore designed also an injector with transonic position of the exit holes with basically the same outer shape and number and dimensions

as the circular holes in the supersonic injector. The transonic injector is shown in **Fig. 6**. The function of the injector was also checked by the CFD modeling.

Only the new supersonic injector with the oval holes was experimentally tested by now.

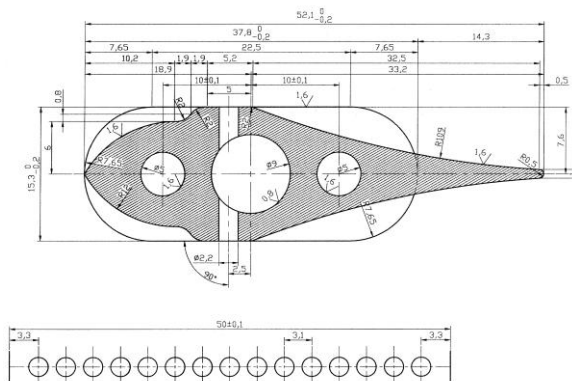


**Fig. 6.** Drawing of the transonic injector

## 4. Design and manufacturing of new solid I<sub>2</sub> evaporator

### 4.1. Evaporator hardware

Molecular iodine dissociated by the RF discharge was examined as another donor of atomic iodine. For this purpose, a new evaporator was designed and manufactured for evaporation of solid state I<sub>2</sub>, and incorporated into the DAIG system including necessary accessories described below. This system for I<sub>2</sub> handling was designed for a long term, stable operation, and to avoid some problems connected with usage of molecular iodine in the COIL/DOIL operation (e.g. unstable iodine vapor flow rate, bad controlling the flow rate, etc.). Such I<sub>2</sub> evaporator was missing in our laboratory.

Main components of the system are: the evaporator, heat exchanger, iodine measuring cell, gas handling piping connected with iodine injector, and water handling hoses. The evaporator is composed of two large-diameter disks (298 mm in active diameter) screwed together, made of pure aluminum (Al 99.5 %), which is sufficiently resistive against iodine corrosion and has excellent heat conductivity. The bottom disk contains a set of concentric circular grooves for filling them with solid I<sub>2</sub>, while the top disk is flat. The bottom disk grooves have a width/depth of 5/5 mm, and their mutual separation is 2 mm. A free space height between the disks is 5 mm. The manufactured evaporator disk with circular grooves and the same disk filled with I<sub>2</sub> are shown on **Photo 3 a, b**. This arrangement is advantageous for uniform iodine heating, and it also prevents formation of large iodine lumps. The evaporation area is surrounded by a circular duct (rectangular cross section 10×10 mm) with 40 small grooves 0.5×1.6 mm distributed periodically around the perimeter. The circular duct serves to equalize pressure around the perimeter. The small grooves serve for a radial injection of a carrier gas (argon was used up to now) from the disk perimeter to the disk center. The

radial gas flow carries the iodine vapor to the central part of the evaporator. Both the bottom and top evaporator disks are equipped with water jackets made of hard aluminum. They hold a hot water flow for heating the evaporator body to desired temperature. The whole evaporator is kept in a Teflon jacket for thermal insulation.



**Photo 3.** Bottom disk of the I<sub>2</sub> evaporator; without solid I<sub>2</sub> (a), with I<sub>2</sub> in the grooves (b)

The external heat exchanger is formed by a 6 m long stainless steel pipe of ¼” in diameter, looped by a heating wire, delivering up to 1500 W. Using inlet cold/hot water and adjusting the flow rate of water, the heat exchanger can deliver hot water for heating the I<sub>2</sub> evaporator in the range of 20-85°C. The water handling hoses between the heat exchanger and the iodine evaporator are thermally insulated by double wall arrangement. Both the pipes are made of the PFA (perfluoralkoxy) Swagelok hoses ¼” and 3/8” in diameter.

The I<sub>2</sub> vapor mixed with buffer gas is introduced into the cell for measuring the I<sub>2</sub> concentration by means of the absorption spectroscopy using Ar<sup>+</sup> laser at 488 nm using the absorption cross-section  $\sigma = 2.47 \times 10^{-18} \text{ cm}^2 \text{ molec}^{-1}$  and a photodiode. The cell is made of pure aluminum (Al 99.5%) and is equipped with two quartz optical windows. The absorption space is formed by a cylinder of 6 mm in diameter and the absorption length is 40 or 25 mm. The measuring cell has four ports, i.e. two for gas inlet/outlet and two for the pressure and temperature measurement.

The I<sub>2</sub> measuring cell and the pipes connecting the evaporator outlet with inlet into the iodine injector in the laser are looped by a heating wire to prevent I<sub>2</sub> precipitation. The iodine injector described in chapter 2 is heated by hot water leaving the water jacket of the evaporator.

Installation of the I<sub>2</sub> evaporator in the DAIG device is shown in **Photos 4, 5**, and the cell for I<sub>2</sub> measurement in **Photo 6**.



**Photo 4.** I<sub>2</sub> evaporator (description in the text above)

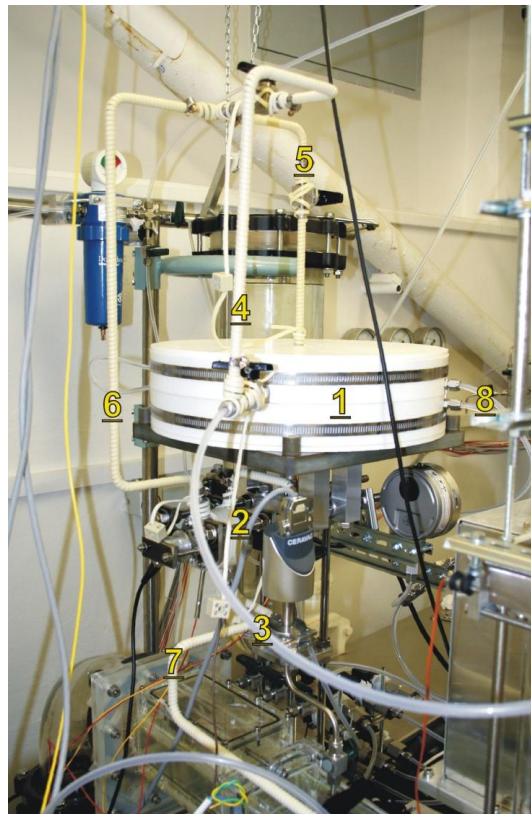


**Photo 5.** I<sub>2</sub> evaporator incorporated in the DAIG device

1 – I<sub>2</sub> evaporator, 2 – I<sub>2</sub> measuring cell, 3 – Ar carrier gas supply, 4 – Ar carrier gas by-pass,  
5 –outlet of I<sub>2</sub> vapor + Ar mixture, 6 – pipe to measuring cell, 7 – pipe from measuring cell to iodine injector,  
8 – heating and/or cooling water input/output

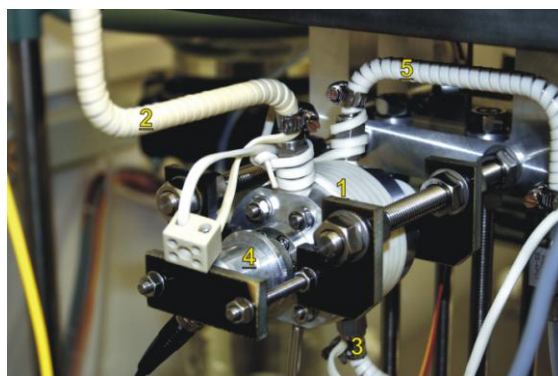


**Photo 6.** Cell for I<sub>2</sub> concentration measurement

1 – I<sub>2</sub> measuring cell, 2 – gas inlet, 3 – gas outlet, 4 – photodiode, 5 – pressure gauge port

#### 4.2. Operation of I<sub>2</sub> evaporation system

Before employing the new I<sub>2</sub> evaporator in the experiments with atomic iodine generation, a testing of its function was performed in the following way. The hot water supply having approx. 50°C was fed to the heat exchanger. Using a heating power of 675 W and water flow rate approx. 12 ml/s, it took about 1 hour to reach 60°C temperature of the aluminum iodine evaporator. After that, increasing to 1330 W and continuously decreasing water flow rate up to 5 ml/s, additional 1 hour was required to reach 79°C. In another experiment, 86°C was attained with 1450 W. We expect that after some experience this temperature could be obtained after 2 hours of heating. With a nearly full heating power (1500 W), the evaporator temperature may be quite conveniently controlled by adjusting the hot water flow rate. A rate of the temperature change is however given by the large thermal persistence of aluminum evaporator. A fast decrease in the evaporator temperature may be also obtained by switching to a cold water supply. The operation of the heat exchanger was not fully optimized yet.

The iodine vapour flow rate from the evaporator was very sensitive to the argon flow rate. An increase in the Ar flow resulted in decreasing in the I<sub>2</sub> flow and vice versa. This fact can be easily explained by variation in pressure inside the evaporator by Ar flow rate, since the mixed flow is choked in the atomic iodine injector. A temporal stability of the I<sub>2</sub> flow rate was very good. An example of the time dependence of I<sub>2</sub> and Ar flow rates is shown in **Fig. 7**.

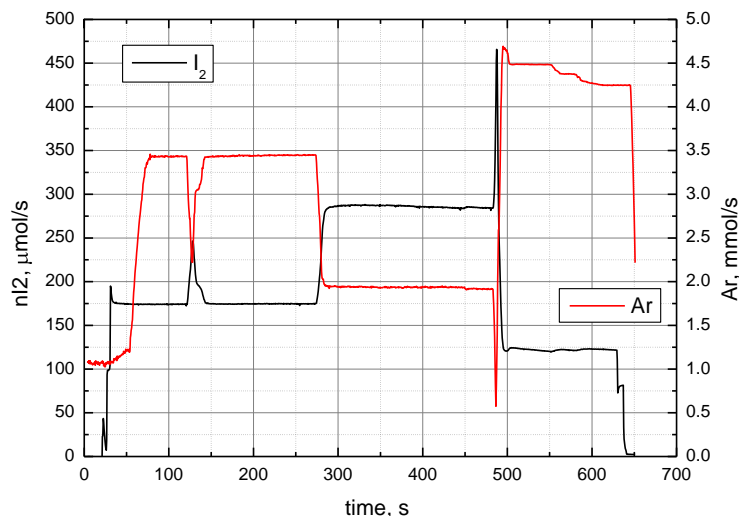


**Fig. 7.** Time dependence of  $I_2$  and Ar flow rates; evaporator temperature  $85^\circ\text{C}$

Dependence of the  $I_2$  flow rate on the Ar flow rate and evaporator temperature is shown in **Fig. 8**.

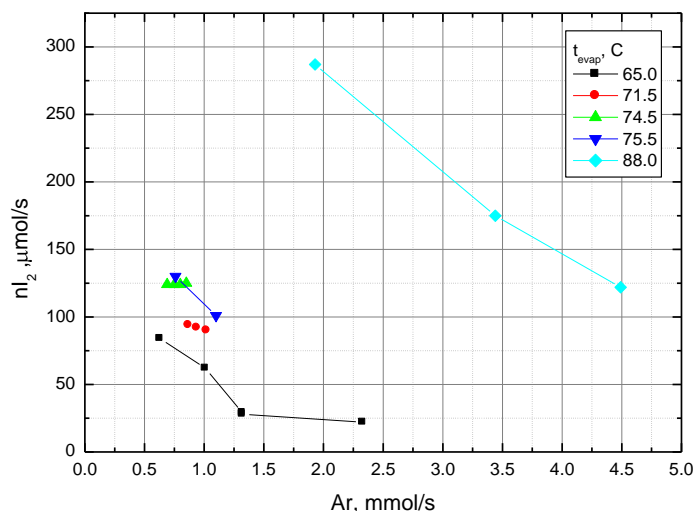


**Fig. 8.** Dependence of  $I_2$  on Ar flow rate and evaporator temperature

The highest  $I_2$  flow rate used in the experiments was  $0.287\text{ mmol/s}$  at  $85^\circ\text{C}$  and  $1.93\text{ mmol/s}$  Ar. We believe that this is not the upper limit, since the temperature may be still increased (perhaps to  $90^\circ\text{C}$ ) and the pressure losses on the way from the evaporator to the injector may be also decreased (the pressure in the iodine cell was  $12\text{ kPa}$  in the highest  $I_2$  flow rate). The heat exchanger may be also modified to use superheated water under the pressure of  $6\text{ bar}$  with  $t > 100^\circ\text{C}$ . A significant improvement in the evaporation rate is expected by replacing the argon with helium, having higher thermal conductivity and lower molecular weight.

## 5. Theoretical background for evaluation of experimental results

Data recorded by the diode probe laser diagnostics (ISD) each 0.15 s were filtered to reduce signal noise and smooth the shape of baseline by moving average over 3-10 subsequent records. For this purpose the IIR (Infinite Impulse Response) function in LabView was employed. Filtered data were further fitted by Voigt profile using the developed Origin script, which combined Origin Peak fitting module with fixed parameter  $wL$  and following expressions

$$T = \left( \frac{wG}{14.49} \right)^2 \quad (1)$$

$$wL = w_{las} + \frac{296}{T} \cdot p \cdot \gamma \quad (2)$$

which relate the Lorentzian and Gaussian width. Here  $T$  is the temperature to be evaluated,  $p$  is the measured cavity pressure,  $w_{las} = 2.5$  MHz is the laser line width, and  $\gamma$  is the  $I(^2P_{1/2}) - I_2(^2P_{3/2})$  broadening coefficient for the gas mixture. The following iterative procedure was used. After an initial estimate of  $wL$ ,  $T$  was calculated from the fitted  $wG$  of the resulted Voigt curve, and with this  $T$  value, a new  $wL$  was calculated from (2). Using the previous initial and present  $wL$  values, a new estimate of  $wL$  was calculated by the bisection method. These iterations were terminated by a difference of two subsequent values of  $wL$  or  $wG$  less than 0.01%. Then the iodine number density from the peak area and the temperature from  $wG$  in the cavity were calculated.

Atomic iodine concentration and temperature measured in the expansion cavity perpendicularly or along the injector were used to evaluate the partial pressure of atomic iodine by the formula

$$p_I = \frac{1}{y_2 - y_1} \int_{y_1}^{y_2} c_I(y) RT(y) dy \quad (3)$$

where  $c_I(y)$ ,  $T(y)$  are the measured concentration and temperature, and  $y$  is the position in direction perpendicular or along the injector. The measurements were performed at a distance of 37-145 mm downstream of the nozzle throat.

The dissociation fraction of iodide RI was evaluated using the formula

$$\eta_{diss} = \frac{p_I}{p_{cav}} \frac{\dot{n}}{\dot{n}_{RI}} \times 100\% \quad (4)$$

where  $\dot{n} = \dot{n}_{Ar} + \dot{n}_{He} + \dot{n}_{N_2} + \dot{n}_{RI}$  is the total gas flow rate, and  $p_{cav}$  is the pressure in the detection cavity. Another important parameter was used, the specific energy,  $E_{sp}$ , defined as

$$E_{sp} = P_{RFabs} / \dot{n}_{RI} \quad (5)$$

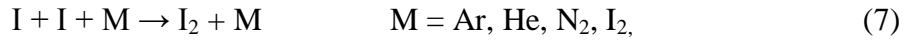
where  $P_{RFabs}$  is the RF power absorbed in the plasma during the RI dissociation.

Efficiency of the dissociation process was evaluated also as a fraction of the absorbed RF power consumed for the RI dissociation,

$$fP_{diss} = \frac{P_{diss}}{P_{abs}} = \frac{e\dot{N}_I E_{bond}}{P_{abs}} \quad (6)$$

where  $E_{bond}$  is the dissociation energy of C-I bond (2.47 eV/molec for CH<sub>3</sub>I, and 2.34 eV/molec for CF<sub>3</sub>I),  $\dot{N}_I$  is the evaluated flow rate of generated iodine atoms (in at/s), and  $e$  is the electric charge of electron. In the case of I<sub>2</sub>, the value of  $E_{bond} = 1.53$  eV/molec must be divided by 2, in order to use the parameter  $fP_{diss}$  consistently.

From the kinetic point of view, the produced iodine atoms by RF plasma dissociation can recombine on the way from the injector to the detection place in reactions



The evaluated I atom number density can be further decreased by eventual presence of the excited iodine atoms since the ISD-based diagnostics monitored the I-I\* transition. For this reason, the  $\eta_{diss}$  values may be considered as a lower limit of the dissociation fraction achieved in the discharge.

## 6. Results of investigation of several atomic iodine donors

### 6.1. Investigation of alkyl iodides CH<sub>3</sub>I and CF<sub>3</sub>I dissociation

#### 6.1.1. Measurements in CW RF discharge; injector with circular injecting holes used

A few examples of experimental results measured in the initial period of this research on the device with the iodine injector having circular injection holes (see Fig. 2) are shown for a typical gas flow and discharge conditions. Most the experimental results were very similar for both alkyl iodides, so the experimental dependence for one of them is usually illustrated. A distribution of atomic iodine concentration, [I], across the measuring cavity for subsonic and supersonic flow conditions for CF<sub>3</sub>I is shown in **Fig. 9**, and recorded by moving the ISD probe beam on the cavity top along the injector axis for CH<sub>3</sub>I is shown in **Fig. 10**.

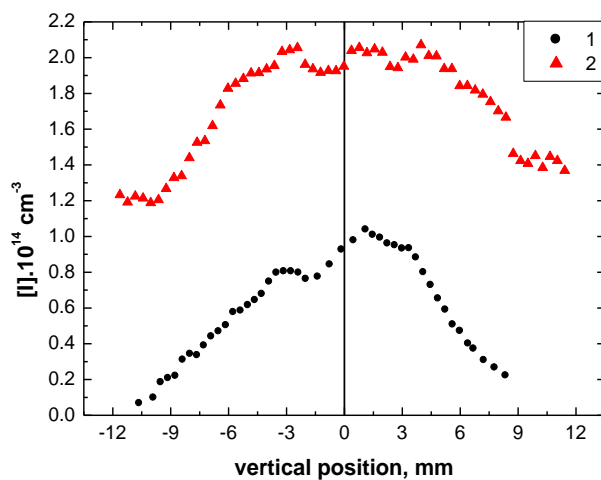


**Fig. 9.** Vertical profile of I number density measured 87 mm downstream of the nozzle throat **1 - supersonic flow** in cavity and  $p = 135$  Pa; **2 - subsonic flow** and  $p = 630$  Pa;  $P_{\text{RF,abs}} = 149$  W; flow rates (mmol/s): 0.28  $\text{CF}_3\text{I}$ , 2.6 Ar, 17  $\text{N}_2$

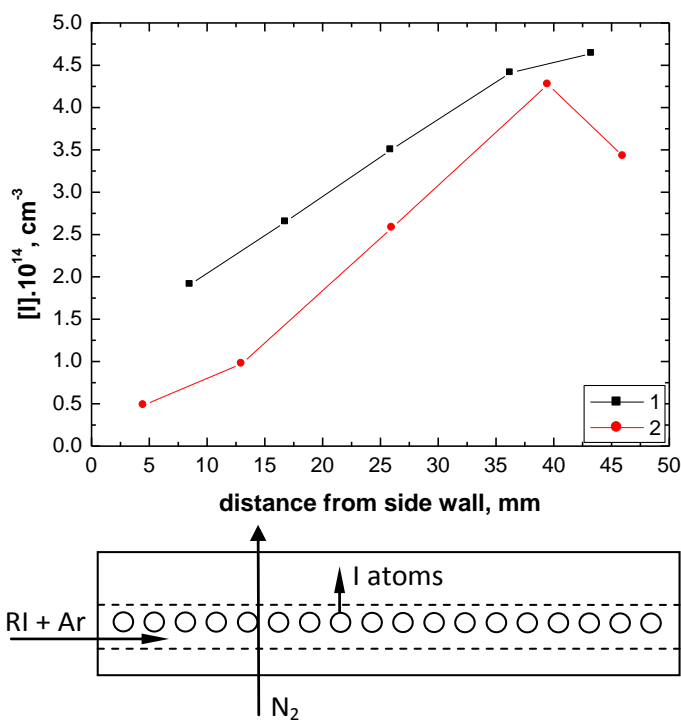


**Fig. 10.** Profile of atomic iodine concentration in direction of the injector axis, measured 87 mm from the nozzle throat; **two different lengths of RF electrodes** used: **1 - 105 mm, 2 - 60 mm**; Conditions: flow rates (mmol/s): 0.51  $\text{CH}_3\text{I}$ , 2.0 Ar, 20  $\text{N}_2$ ,  $p_{\text{cav}} = 600$  Pa,  $P_{\text{RF,abs}} = 150$  W

Dependences in Fig. 9 demonstrated that  $[\text{I}]$  was much lower in the supersonic flow than in the subsonic flow, but the dissociation fraction was almost independent on the cavity pressure and distance from the nozzle throat. A monotonic increase in  $[\text{I}]$  in Fig. 10 from the side of  $\text{CH}_3\text{I}$  inlet into the discharge chamber (i.e., from the first injector holes to the last one) was ascribed to an

increase in the flow gas residence time through the injector. In these experiments, an effect of variable length of the RF electrode (60 mm and 105 mm) inserted in the discharge cavity was also tested, and it can be seen that the curve (1) corresponding to a longer electrode starts at higher [I] values than the curve (2) for a shorter electrode. Observed increase in [I] was in accordance with observed much stronger plasma afterglow leaving the holes at the most distant holes from CH<sub>3</sub>I inlet.

Dependences of the dissociation fraction on specific energy,  $E_{sp}$ , for several CH<sub>3</sub>I and CF<sub>3</sub>I flow rates, measured with two lengths of RF electrodes and different RF power are shown in **Figs. 11 a, b**.

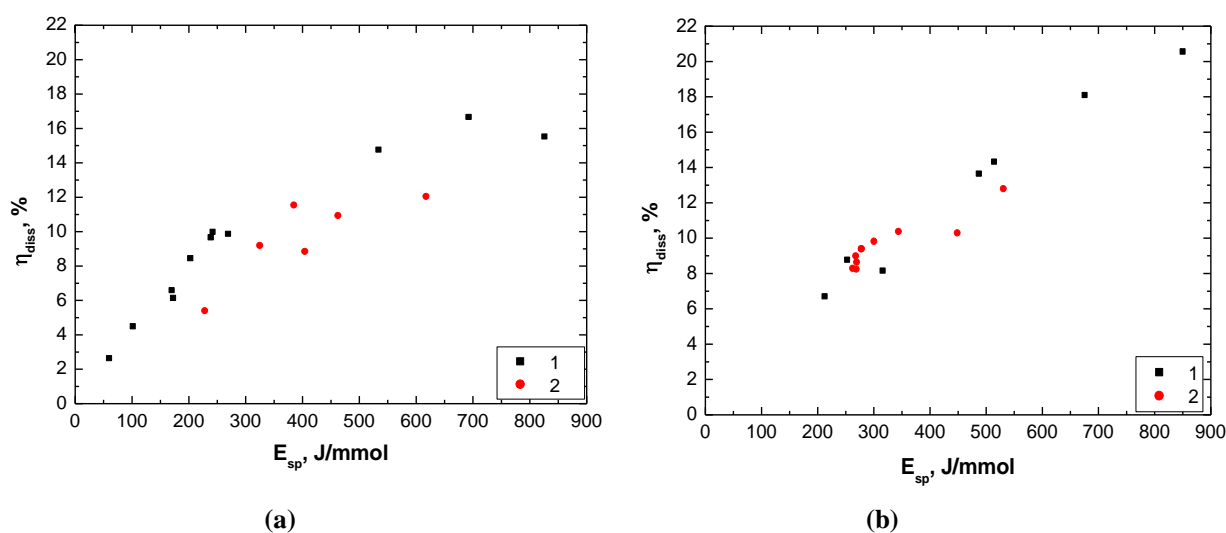


**Fig. 11 a, b.** Dissociation fraction of **CH<sub>3</sub>I (a)** and **CF<sub>3</sub>I (b)** in dependence on specific energy  $P_{RF,abs} = 100-250$  W;  $L_{electrode} = 105$  mm (1) or 60 mm (2); flow rates (mmol/s): 0.1 - 0.72 CH<sub>3</sub>I, 0.28/1.0 CF<sub>3</sub>I, 1.9 - 2.7 Ar, 16 - 20 N<sub>2</sub>

In case of CH<sub>3</sub>I, one can see a certain saturation, which is shifted to a lower  $E_{sp}$  value for the shorter electrode. This effect may be explained by a higher power density because the plasma is in a smaller volume at the same RF power. Despite of the 1.75times higher power density in case of using the shorter electrode, the dissociation fraction was lower. In the linear region of dependences (i.e. prior to saturation with CH<sub>3</sub>I), the dissociation fraction was nearly the same for both donors. In case of CF<sub>3</sub>I, no saturation was observed using both the longer and shorter electrode.

The RI dissociation efficiency expressed by the dependence of fraction of the RF power absorbed (consumed) in the dissociation process of CH<sub>3</sub>I and CF<sub>3</sub>I on the specific energy  $E_{sp}$  is shown in **Fig. 12 a, b**. It can be seen that CH<sub>3</sub>I exhibits a steeper decrease in this dependence than CF<sub>3</sub>I, and results with CF<sub>3</sub>I were also less sensitive to the electrode length.

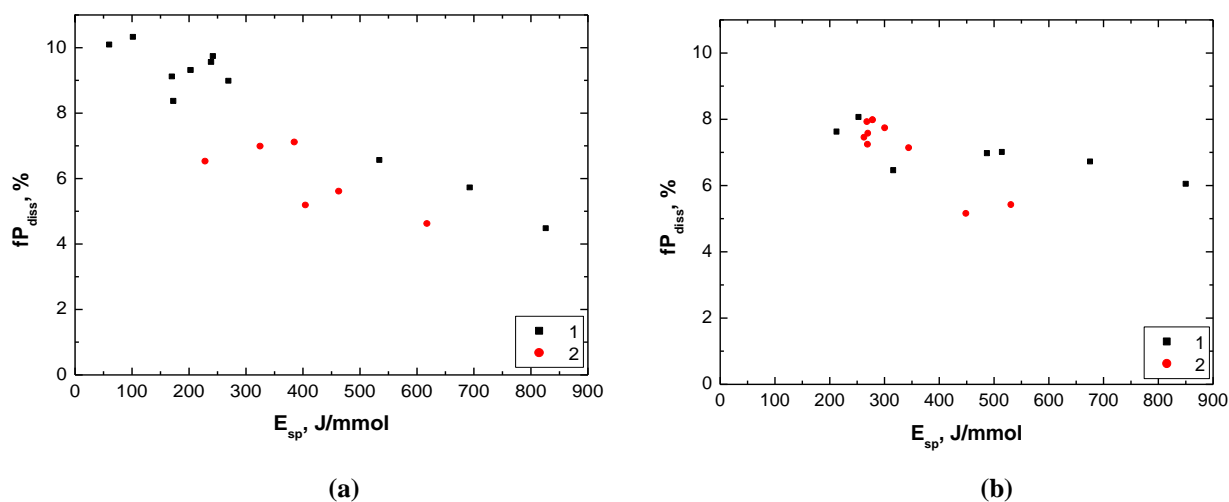


**Fig. 12 a, b.** Fraction of RF power consumed for  $\text{CH}_3\text{I}$  (a) and  $\text{CF}_3\text{I}$  (b) dissociation in dependence on specific energy

$P_{\text{abs}} = 100\text{-}250$  W;  $L_{\text{electrode}} = 105$  mm (1) or 60 mm (2);  
 flow rates (mmol/s): 0.1 - 0.72  $\text{CH}_3\text{I}$ , 0.28/1.0  $\text{CF}_3\text{I}$ , 1.9 - 2.7 Ar, 16-20  $\text{N}_2$

Static temperature evaluated from the ISD probe recoding across the measuring cavity is shown in Fig. 13.

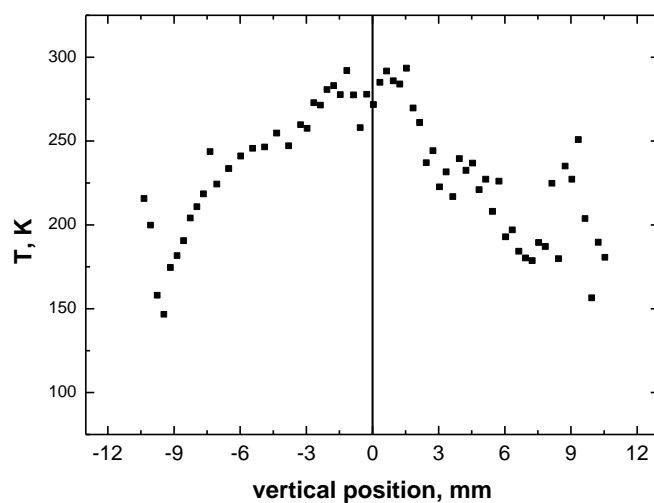


**Fig. 13.** Vertical profile of static temperature, record 87 mm from the nozzle throat

$L_{\text{electrode}} = 60$  mm;  $p_{\text{cav}} = 128$  Pa,  $P_{\text{RF, abs}} = 148$  W;  
 flow rates (mmol/s): 0.3  $\text{CH}_3\text{I}$ , 2.7 Ar, 17  $\text{N}_2$

**Discharge stability in the gas mixture containing the alkyl iodides was a serious problem solved during this research period.** Several possibilities of its improvement were examined. One of them was adding a small amount of NO (100-600  $\mu\text{mol/s}$ ) or  $\text{N}_2$  (50-1300  $\mu\text{mol/s}$ ) into the RI + Ar mixture, however no evident increase in the RF discharge performance was observed at the employed gas flow and discharge conditions.

Important enhancement in the discharge stability with  $\text{CH}_3\text{I}$  was achieved by covering the RF tungsten electrode (95 mm long) with a thin quartz glass tube, which served as a dielectric cover. In this way, the absorbed CW RF power could be increased up to 350 W (the previous limit was ~150-250 W) and the maximum attained dissociation fraction thus increased from ~16% to 23%. By employing a repetitively pulsed mode of the RF source with 20 kHz frequency and a pulse duty ratio 90% (see chap. 6.1.3.), a maximum possible instantaneous RF power of 500 W could be used (the absorbed power was  $P_{\text{RF,abs}} = (P_{\text{inst}} - P_{\text{reflected}}) \times (\text{p.d.r.}) = (500 - 40) \times 0.9 = 414 \text{ W}$ ) at up to 0.66  $\text{CH}_3\text{I}$  mmol/s. Unfortunately, after several minutes of the DAIG operation, the quartz tube on the electrode was covered with a thin layer of carbon deposit.

Another improvement of the discharge instability was realized by a special element inserted into the gas inlet hole of the discharge cavity, which forced the RI+Ar mixture to a tangential flow and making a vortex in the discharge chamber. By using this element, the highest absorbed RF power (440 W) and the dissociation fraction of 23% at 0.66 mmol/s of  $\text{CH}_3\text{I}$  was attained. Atomic iodine with a flow rate of 0.15 mmol/s was produced, which was 1.5times more than the best value obtained before the improvements.

**Fig. 14** summarizes results on the dissociation fraction of  $\text{CH}_3\text{I}$  obtained with above described hardware modification to increase the RF discharge stabilization. It is evident that most efficient was the tangential gas inlet into the discharge chamber.

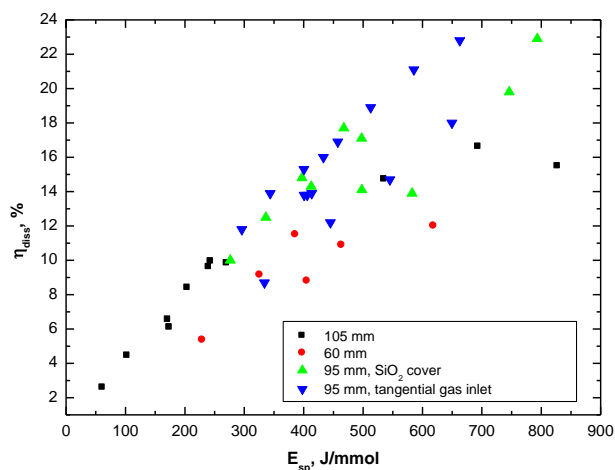


**Fig. 14.** Dissociation fraction of  $\text{CH}_3\text{I}$  in dependence on the specific energy for different hardware configurations; measured 87 mm from the nozzle throat; flow rates (in mmol/s): 18-21  $\text{N}_2$ , 2-2.5 Ar;  $p_{\text{cav}}$  500-900 Pa

### 6.1.2. Measurements in CW RF discharge; injector with oval injecting holes used

Experimental **results on CF<sub>3</sub>I dissociation** measured with the modified iodine injector with oval injection holes (see chap 3, Fig. 4) for supersonic iodine injection are further presented. It was found that the discharge stability was significantly better in comparison with experiments performed with the former injector type (with circular holes). The RF frequency was maintained at 40 MHz, and the RF rod electrode 95 mm long without the quartz glass cover was used. In comparison with the previous limit of the RF power of 250 W, the discharge up to the RF source power limit (500 W) could be maintained at a broad range of CF<sub>3</sub>I flow rate 0.1-0.9 mmol/s, and Ar flow rate 1.3-3.7 mmol/s. Thanks to a larger cross-section of the injection holes, the discharge pressure was by about 20% lower than in the former injector.

A vertical profile of generated atomic iodine number density was recorded by the ISD with the probe beam led perpendicularly to the supersonic flow 65 mm downstream of the nozzle throat. Results of these measurements for 0.8 mmol/s of CF<sub>3</sub>I, 3.12 mmol/s of Ar, and two values of the RF power are shown in **Fig. 15**.

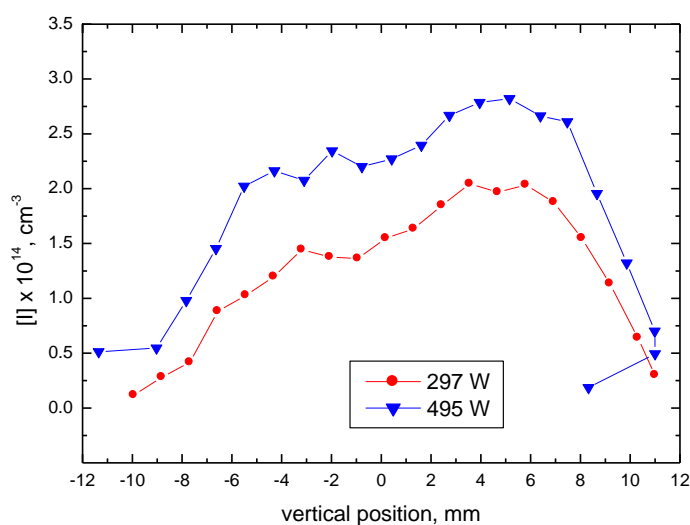


**Fig. 15.** Vertical profile of I number density measured 65 mm downstream of the nozzle throat  
Flow rates (mmol/s): 0.8 CF<sub>3</sub>I, 3.12 Ar, 19.9 N<sub>2</sub>, p<sub>cav</sub> = 135 Pa

The asymmetry of the measured curves was permanent, and may be caused by a buoyancy effect.

The temperature evaluated from the broadening of the absorption peak for the same conditions is shown in **Fig. 16**.

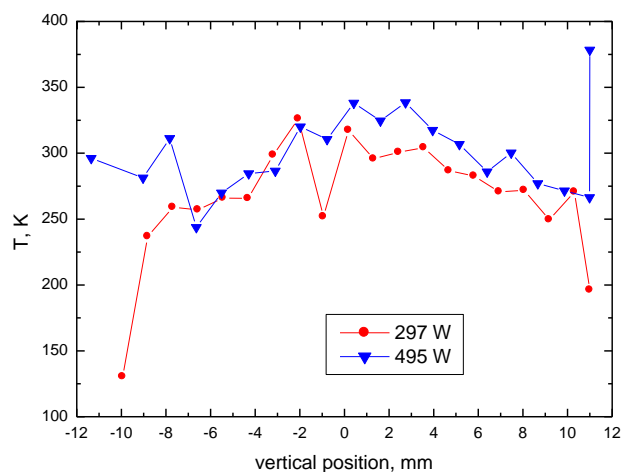


**Fig. 16.** Vertical profile of temperature measured 65 mm downstream of the nozzle throat  
Conditions as in Fig.15

Note that even minimum value of temperature in the supersonic flow is higher than 240 K at high  $\text{CF}_3\text{I}$  flow rate (0.8 mmol/s) and absorbed RF power (495 W). The temperature averaged across the cavity was dependent both on the RF power and  $\text{CF}_3\text{I}$  flow rate – see **Fig. 17**.

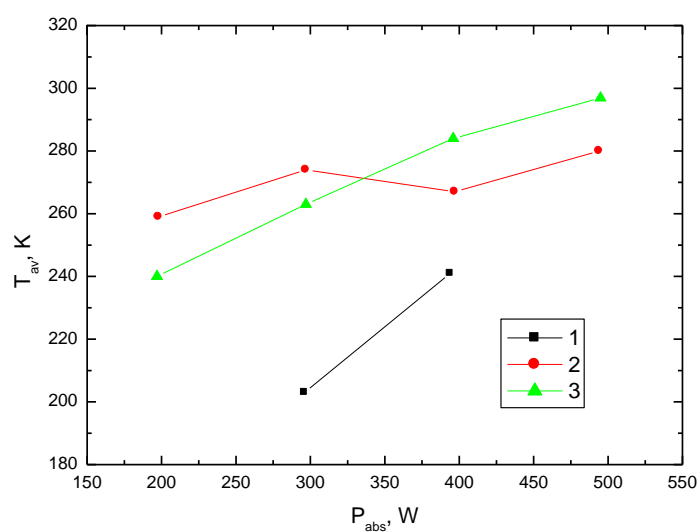


**Fig. 17.** Average temperature in dependence on the absorbed power  
Flow rate of  $\text{CF}_3\text{I}$  (mmol/s): 0.33 (1), 0.50 (2), 0.80 (3); other conditions as in Fig.15.

The iodine concentration was quite constant along the gas flow in the measuring cavity because no difference was recorded when the probe beam was moved from the distance of 65 mm to 115 mm downstream from the nozzle throat.

A relatively high dissociation fraction of 38.7% was recorded at 397 W but with 0.06 mmol/s of  $\text{CF}_3\text{I}$  only. Atomic iodine production of 0.15 mmol/s was obtained at 495 W with 0.78 mmol/s of  $\text{CF}_3\text{I}$ . A dependence of the produced atomic iodine rate on the absorbed power is shown in **Fig. 18**.

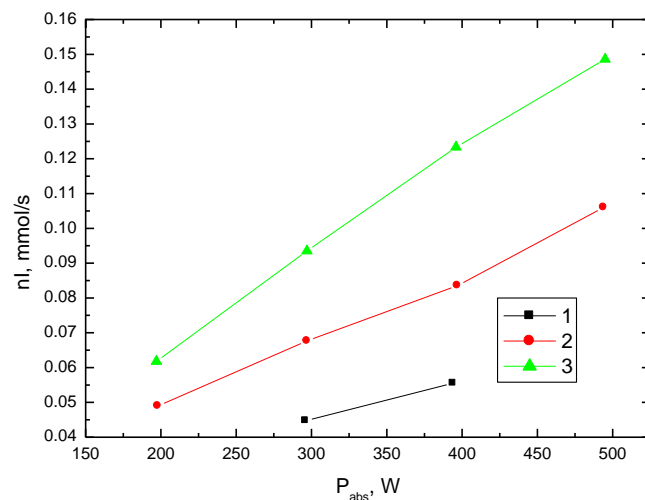


**Fig. 18.** Dependence of the produced atomic iodine rate on the absorbed power  
Conditions as in Fig. 17

Employing a tangential inlet to the injector resulted still in better achieved results. For example, the dissociation fraction was 26% at 0.3 mmol/s of  $\text{CF}_3\text{I}$  and 495 W. The maximum production of I atoms of 0.19 mmol/s was obtained with 0.9 mmol/s of  $\text{CF}_3\text{I}$ , and at 20.6% dissociation fraction and 8.5 % discharge efficiency.

Due to the achieved good discharge stability, we could obtain a very broad dependence of the dissociation fraction and discharge efficiency on the specific energy (from 250 J/mmol to ~5000 J/mmol). These results are plotted together with the former results in **Figs. 19, 20**. The dependencies exhibit a saturation at  $E_{\text{sp}} = 4000$  J/mmol, where the dissociation fraction reached 30%, but the discharge efficiency is below 2%.

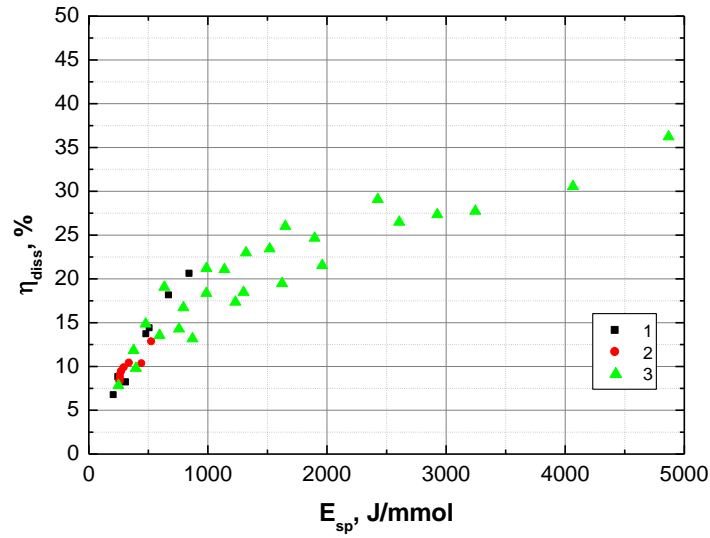


**Fig. 19.** Dissociation fraction of  $CF_3I$  in dependence on specific energy  
Different conditions

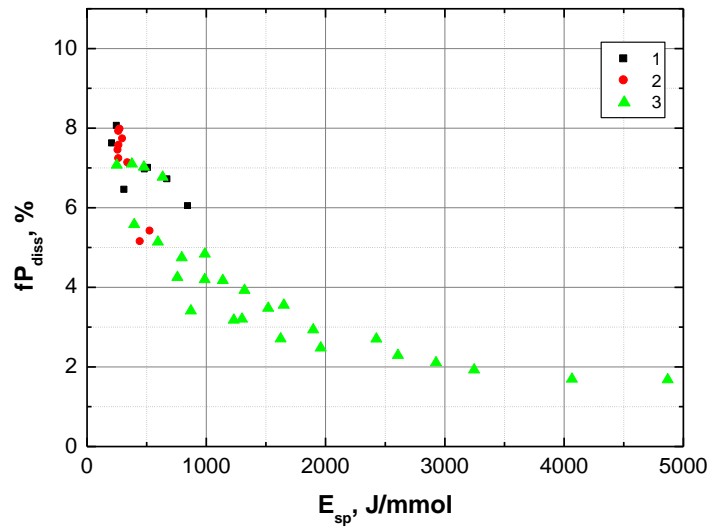


**Fig. 20.** Fraction of RF power consumed in  $CF_3I$  dissociation (i.e., discharge efficiency)  
in dependence on specific energy; different conditions

It is not possible to compare the former and new injector at conditions of the high  $E_{sp}$ , as the data with the former injector could not be measured for these values due to lower discharge stability. For the lower  $E_{sp}$  values, no improvement in the dissociation efficiency was obtained with the new injector. The most probable reason for this fact was a shorter gas residence time in the discharge (the new injector has lower pressure in the discharge space).

### 6.1.3. Measurements in pulse-periodic RF discharge

A few experimental sets were performed with a pulse-periodic RF discharge, during which the basic 40 MHz RF power supply was periodically switched on and off with frequency from 0.7 kHz to 99 kHz. A pulse duty ratio (ratio between “on” time and “off” time in the period) was changed from 10 to 100%. A study of the repetition rate effect and pulse duty ratio on the atomic iodine number density was performed at the cavity center, 47 mm from the injector outlet. The dependence on the repetition frequency for three values of the pulse duty ratio is shown in **Fig. 21**.

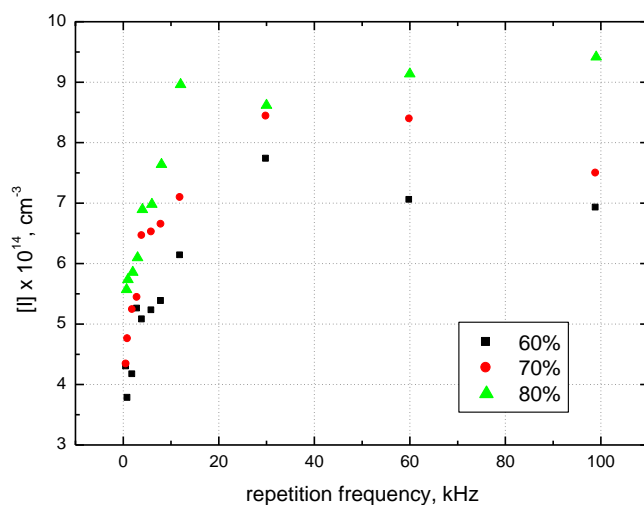


**Fig. 21.** Dependence of I number density on repetition frequency for 3 values of pulse duty ratio, measured 47 mm downstream from the injector outlet;  $p_{\text{cav}} = 960$  Pa; flow rates (mmol/s): 0.72  $\text{CH}_3\text{I}$ , 2.3 Ar, 24  $\text{N}_2$ , RF power 237 W

A weak maximum can be seen around 15 kHz, and the dissociation fraction strongly decreased at frequencies lower than 4 kHz, which roughly corresponded with a gas residence time in the discharge chamber ( $\sim 0.6$  ms).

The repetition frequency had only a weak effect on atomic iodine number density, and in case of  $\text{CF}_3\text{I}$ , a slight improvement of sparking instability of the discharge was observed in comparison with the CW discharge mode at  $f = 30$  kHz. Dissociation fraction and efficiency,  $fP_{\text{diss}}$ , were comparable with the CW mode. No influence on static temperature in the cavity was found when switching from the cw to pulse-periodic mode. These measurements were described in more details in interim report [7].

#### 6.1.4. Post-discharge modeling of recombination

##### a) Modeling of CH<sub>3</sub>I

The evaluated dissociation fraction and consequently the value of dissociation efficiency could be decreased by presence of excited iodine atoms, I\*, and recombination losses (eqs. 7-9). A 3-D CFD modeling of the reactive flow was performed to evaluate the recombination processes by means of the commercial, finite-volumes-code CFD-ACE+ software.

The input molar flow rates were: 20 mmol/s of primary N<sub>2</sub>, 2 mmol/s of Ar as a carrier gas, 0.373 mmol/s of CH<sub>3</sub>I, 0.0746 mmol/s of I, and 0.0746 mmol/s of CH<sub>3</sub>. The dissociation fraction of CH<sub>3</sub>I leaving the discharge and entrancing the injector holes was 20%. Further details are given in the Interim Report 001 [7].

By integrating the species flux over the selected cross-sections, the flow rates of the species relative to the flow rate of CH<sub>3</sub>I entraining the discharge were evaluated. The contours of I<sub>2</sub> mass fraction after I recombination are shown in **Fig. 22**.

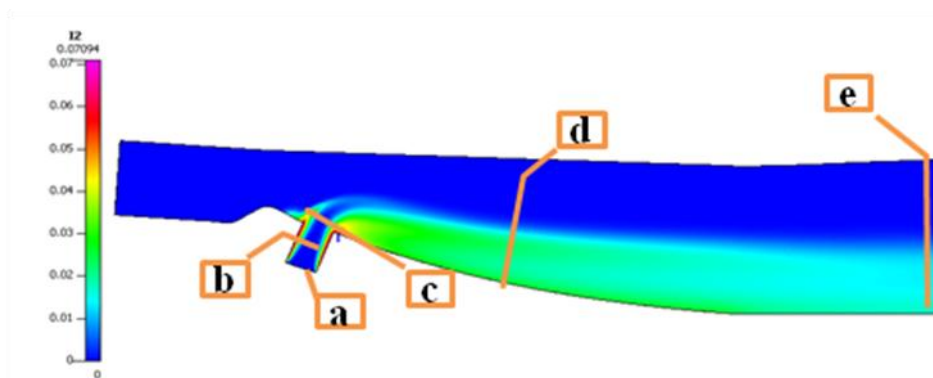


**Fig. 22.** Contours of I<sub>2</sub> mass fraction in different locations of the flow cavity

A plot of averaged flow rates of species related to the input CH<sub>3</sub>I number density can be seen in **Fig. 23**.

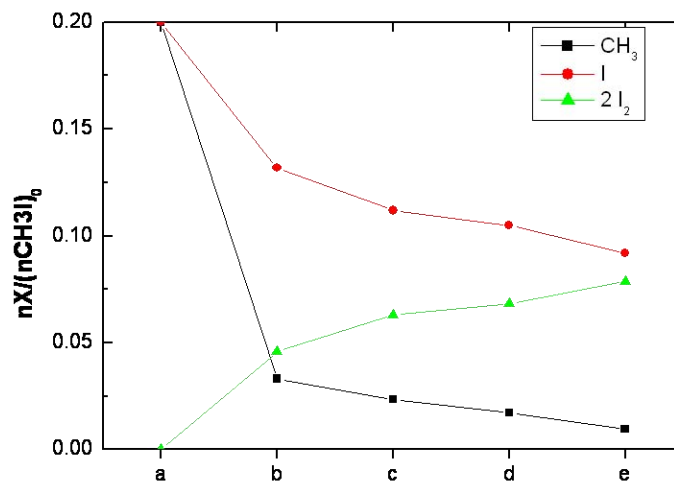


**Fig. 23.** Modeling of recombination processes in discharge decomposition of CH<sub>3</sub>I (see Fig. 22)

It is obvious from these results that nearly 50% of produced atomic iodine was recombined on the gas mixture passage through the 3 mm-injector hole. The most effective process was the wall recombination. The recombination to CH<sub>3</sub>I contributed to the total recombination loss by 1/3, and I recombination in a triple process (7) was of minor importance. The calculations also revealed that CH<sub>3</sub> radical was very fast recombined to dimer C<sub>2</sub>H<sub>6</sub>, which is very exothermic process (-375.2 kJ/mol), very probably responsible for quite high temperature in the supersonic cavity. The mutual reaction between two CH<sub>3</sub> or CF<sub>3</sub> radicals is otherwise advantageous for inhibition of recombination of I atoms in the process (9).

### b) Modeling of CF<sub>3</sub>I dissociation

A simplified plasma-kinetic model was used for calculation of the CF<sub>3</sub>I dissociation. A simple Global kinetic model [16] was used, which does not count for a spatial distribution of species in direction perpendicular to the electrodes. This assumption is well satisfied in a high pressure glow discharge, since the sheath layers at the electrodes are very thin. The axial spatial distribution is calculated from a time evolution of the solved kinetic equations. The rate constants and collision cross-sections were taken from Ref. [17], and the recombination of radicals  $2 \text{CF}_3 \rightarrow \text{C}_2\text{F}_6$  was added.

Due to assumption of some elementary process rates, e.g. cross-sections of the iodine production from excited states of CF<sub>3</sub>I, our calculations should be treated as very approximate and only qualitative results are mentioned: (i) Enhancement of the dissociation fraction by decreasing discharge pressure seemed to be very large. (ii) Pure Ar buffer was better than Ar + He mixture used as a carrier gas since increasing  $p_{\text{Ar}}$  provided more electrons, while increasing  $p_{\text{He}}$  caused only a higher recombination (confirmed by experiments). (iii) Electron temperature was 2-3 eV, and

plasma density  $N_e \sim 10^{12} \text{ cm}^{-3}$ . (iv) Recombination of  $2 \text{ CF}_3 \rightarrow \text{C}_2\text{F}_6$  was effective yet inside the discharge chamber. A time course of relative concentrations of three species is shown in **Fig 24**.

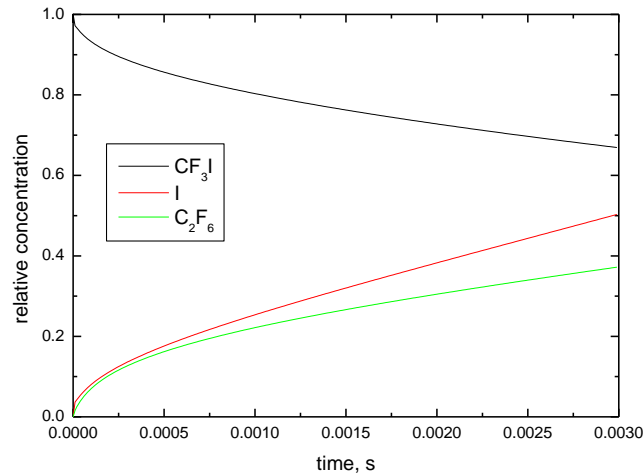


**Fig. 24.** Time course of calculated relative concentrations along the discharge tube

A continuous rise of the iodine concentration after 1 ms (approx. gas residence time in case the 105 mm-electrode) is in accordance with the observed increase in iodine number density measured in the experiments along the injector axis. This result indicated that still a longer discharge tube should be used to achieve higher dissociation fraction under these flow and pressure conditions. More detailed results on this modeling are given in the interim report [7].

## 6.2. Investigation of HI dissociation

The experiments with hydrogen iodide, HI, discharge dissociation were motivated partly by using HI in our previous research on chemical generation of atomic iodine and current research on the all-gas generation of molecular iodine. Investigation of HI dissociation in the DAIG device was performed still before the above described hardware improvements, and with the short (60 mm) RF electrode.

The dissociation fraction and fraction of RF power to dissociation (the discharge efficiency) in dependence on the absorbed CW RF power is shown in **Fig. 25**

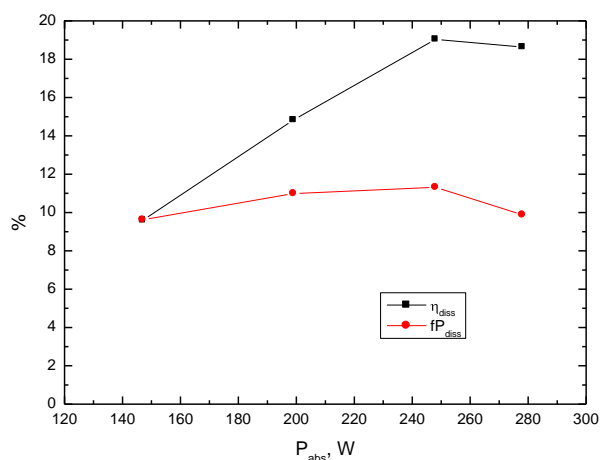


**Fig. 25.** Dissociation fraction of **HI** and discharge efficiency in dependence on the absorbed power; measured 87.5 mm from the nozzle throat; flow rates (mmol/s): 18.1 N<sub>2</sub>, 2.1 Ar, 0.5 HI; p<sub>cav</sub> 551 Pa

Although the dissociation fraction decreased with the HI flow rate, the efficiency slightly increased. These dependencies were measured under subsonic conditions (550-630 Pa) but a few results obtained also under supersonic conditions (126 Pa) were very similar.

For better discharge stability above the RF power of 300 W, most of the experiments were conducted with the pulse-periodic RF discharge (50 kHz, pulse duty ratio 80%). Example of these results is given in **Fig. 26**, showing the dependences of the dissociation fraction, discharge efficiency, and flow rate of produced atomic iodine on the HI flow rate.

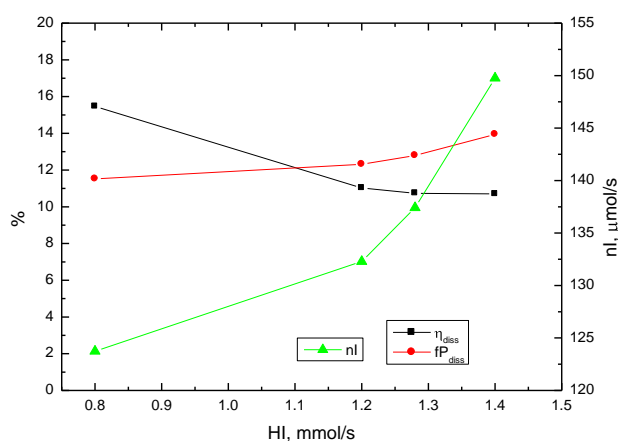


**Fig. 26.** Dissociation fraction of HI, discharge efficiency and flow rate of produced I in dependence on HI flow rate; measured 87.5 mm from the nozzle throat; flow rates (mmol/s): 19.1 N<sub>2</sub>, 3.1 Ar; p<sub>cav</sub> 400-500 Pa; P<sub>abs</sub> 317 W

During these experiments, argon flow rate was also optimized resulting in monotonous increase of the dissociation fraction up to ~18% in the Ar flow rate used range (details in [7]). A horizontal profile of the atomic iodine number density was similar as with CH<sub>3</sub>I and CF<sub>3</sub>I.

Comparison of the dissociation and discharge efficiency of HI and alkyl iodides CH<sub>3</sub>I, CF<sub>3</sub>I is demonstrated in the following **Figs. 27 a, b** (measured under similar discharge conditions).

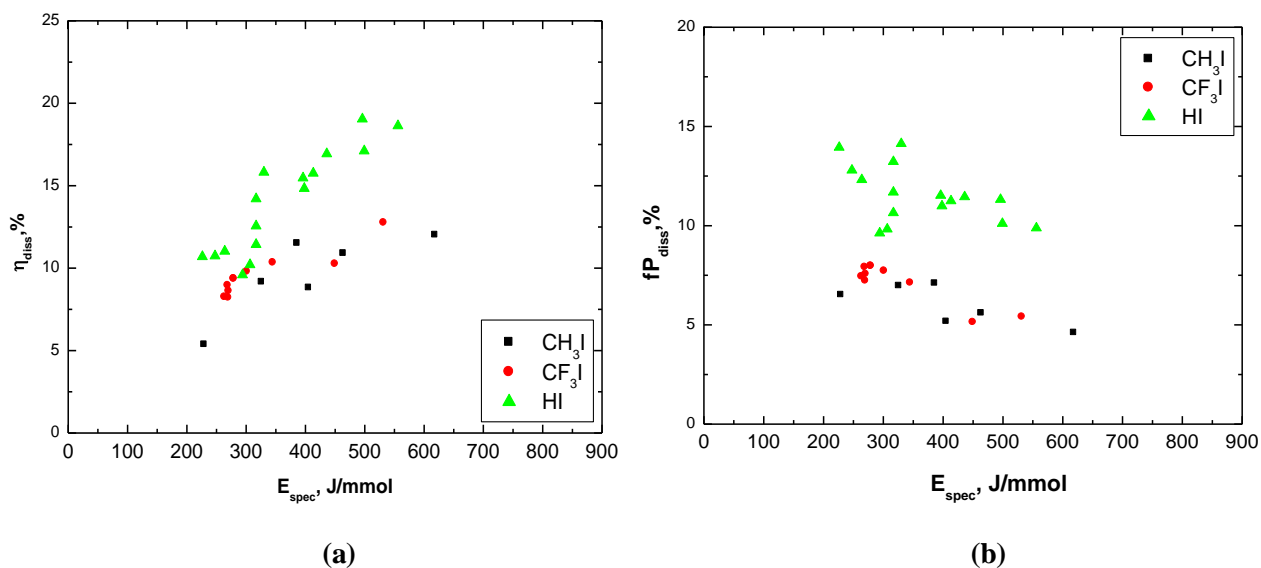


**Fig. 27 a, b.** Dissociation fraction (a), and discharge efficiency (b) of different iodides in dependence on the specific energy; measured in subsonic flow, various conditions

It is obvious that HI provides the best results of these three iodine donors. The efficiency  $fP_{diss}$  is two times higher for HI than for RI, despite a higher iodine bond energy (3.06 eV vs ~2.4 eV for RI). A higher discharge efficiency of HI could be ascribed to its lower recombination rate.

### 6.3. Investigation of I<sub>2</sub> dissociation

Molecular iodine was newly studied as the atomic iodine source. Most of the experiments were conducted under subsonic flow regime, and with N<sub>2</sub> as a primary gas (18-20 mmol/s). The injector with oval holes and 95 mm long RF electrode were used.

In the first two experimental series, the ISD probe beam was led so that the vertical profiles of atomic iodine number density were recorded. The distance from the nozzle throat was fixed at 65 mm through all the experiments. The subsonic vertical profiles for two flow rates of argon (and, consequently, two flow rates of I<sub>2</sub>) are shown in **Fig. 28**.

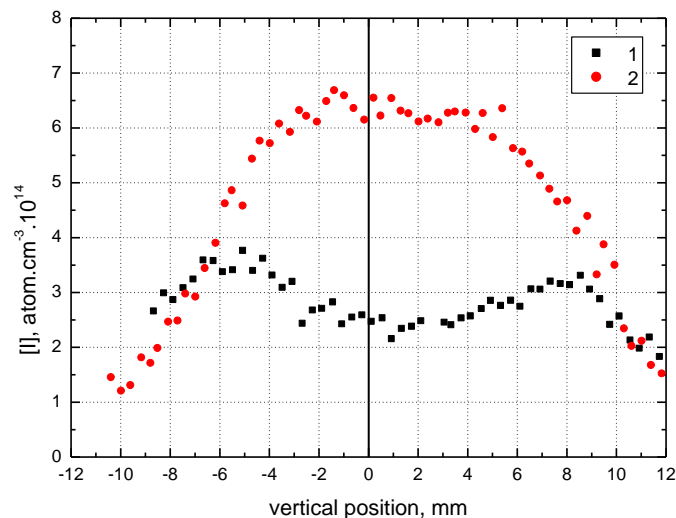


**Fig. 28.** Vertical profiles of atomic iodine number density 65 mm downstream of the nozzle throat  
 Flow rates:  $\text{N}_2$  17.5 mmol/s, Ar 3.37 (1) and 0.64 (2) mmol/s,  $\text{I}_2$  50 (1) and 220 (2)  $\mu\text{mol/s}$ ;  
 pressure in the cavity 317 (1) and 414 (2) Pa, absorbed RF power 199 W (1) and 247 W (2)

The influence of cavity pressure (choking) on the atomic iodine concentration and its distribution is shown in **Fig. 29**.

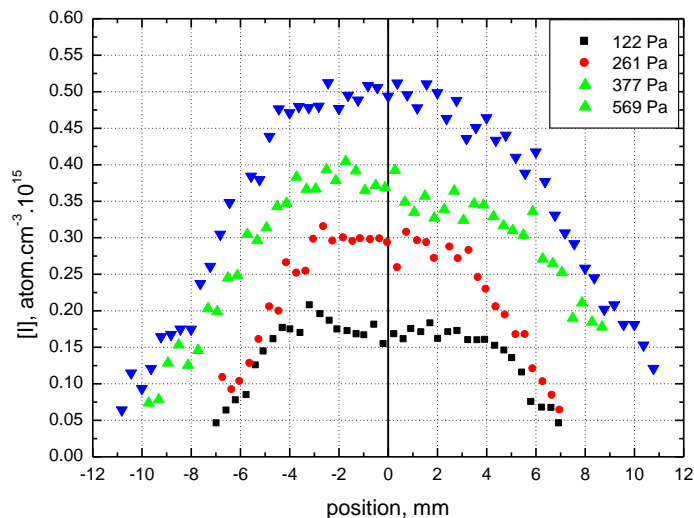


**Fig. 29.** Vertical profiles of atomic iodine number density 65 mm downstream of the nozzle throat for different cavity pressures

Flow rates:  $\text{N}_2$  18.8 mmol/s, Ar 0.69,  $\text{I}_2$  124  $\mu\text{mol/s}$ ,  $P_{\text{abs}}$  195 W.

The dissociation fraction was 30% under these conditions and was independent on the pressure, except of the highest  $p_{\text{cav}} = 569$  Pa, where it decreased to 23%, probably due to the iodine atoms

recombination on the injector outer walls. The lowest pressure  $p_{cav} = 122$  Pa corresponds to the supersonic regime.

The smoothed vertical profiles of the static temperature are shown in **Fig. 30**.

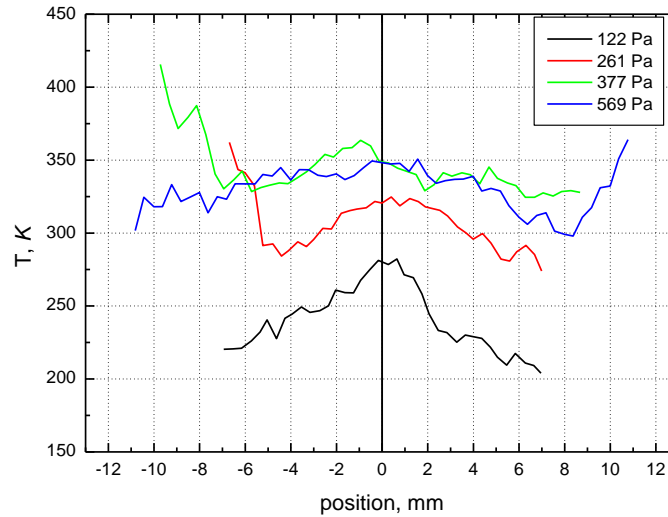


**Fig. 30.** Smoothed vertical profiles of static temperature 65 mm downstream of the nozzle throat for different cavity pressures. Conditions as in Fig. 29

In the supersonic flow experiment, the peak number density was  $2 \times 10^{14} \text{ cm}^{-3}$  and the minimum temperature 210 K. The estimated Mach number from Pitot tube measurement was 1.55.

One experimental series was performed with the “horizontal” ISD scanning, i.e. along the injector at the distance from the nozzle throat 65 mm again. The obtained horizontal concentration profiles were very inhomogeneous – see **Fig. 31**.

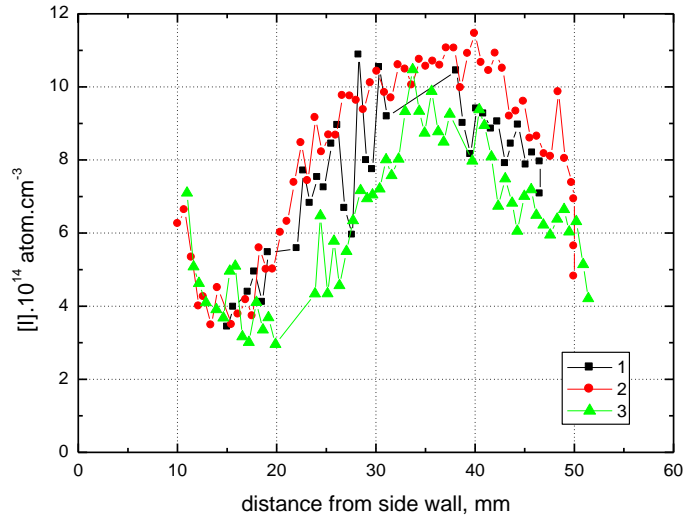


**Fig. 31.** Horizontal profiles of atomic iodine number density 65 mm downstream of the nozzle  
 Flow rates: N<sub>2</sub> 18.9-19.7 mmol/s, Ar 4.25 (1), 3.44 (2), 1.93 (3) mmol/s, I<sub>2</sub> 122 (1), 175 (2), 287 (3) μmol/s,  
 P<sub>abs</sub> 197 W, p<sub>cav</sub> 559 (1), 540 (2), 507 (3) Pa

The shape of the horizontal profile was not affected by either I<sub>2</sub>, or Ar flow rate.

In the following figures, we present summary dependencies of the produced atomic iodine rate, dissociation fractions and discharge efficiencies. The dissociation fraction did not decline below 20% through all experiments. The flow rate of the produced atomic iodine is shown in **Fig. 32**.

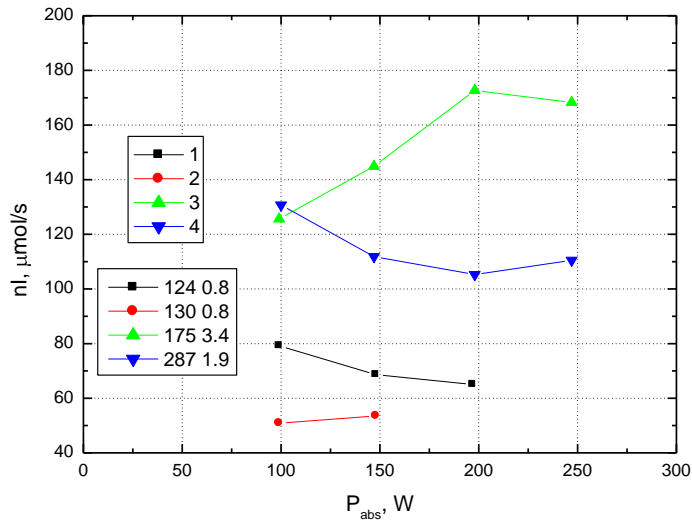


**Fig. 32.** Flow rate of the produced atomic iodine in dependence on the absorbed RF power  
 Flow rates of Ar + I<sub>2</sub> (in mmol/s): 0.8 + 0.124 (1), 0.8 + 130 (2), 3.4 + 0.175 (3), 1.9 + 0.287 (4).  
 N<sub>2</sub> 18.9-19.7 mmol/s, p<sub>cav</sub> 289-778 Pa

The Fig. 32 illustrates also the influence of Ar flow rate on the atomic iodine production. Although the  $I_2$  flow rate was much higher for the curve 4 than for the curve 3, the produced atomic iodine was lower, perhaps due to the lower Ar flow rate. We explain this feature by lower electron density with lower Ar content. The increase in the RF power above 100 W also did not bring more atomic iodine, although the dissociation fraction was only 22.8% at 100 W.

The summary graph of the achieved dissociation fractions is shown in **Fig. 33**.

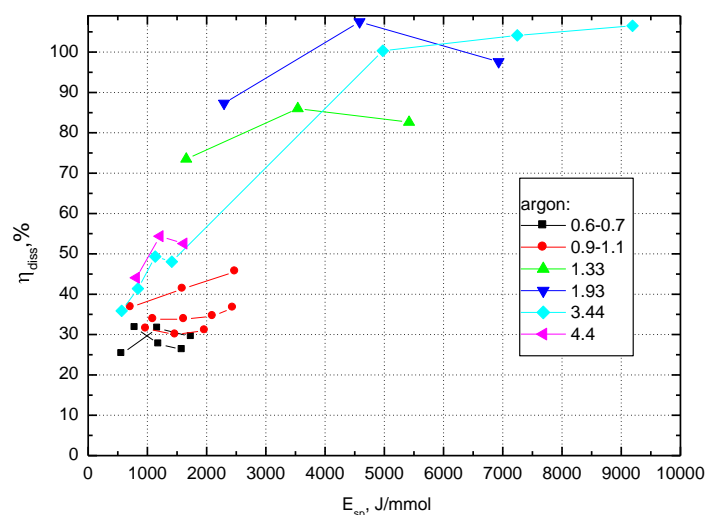


**Fig. 33.** Dissociation fraction of  $I_2$  in dependence on the specific input energy for different Ar flow rates

The data used in this figure comprise the following conditions:  $I_2$  flow rates 22-287  $\mu\text{mol/s}$ ,  $P_{\text{abs}}$  48-247 W, Ar 0.63-4.49 mmol/s,  $N_2$  18.5-19.2 mmol/s and  $p_{\text{cav}}$  122-809 Pa. The points yielding 100% correspond to low  $I_2$  flow rates, 22-28  $\mu\text{mol/s}$ , where there is a relatively large error in the absorption measurement. Therefore some values exceed 100%. The specific energy corresponding to the maximum  $\eta_{\text{diss}}$  (or saturation point) for each curve is shifted to lower values with lower Ar flow rate. The fact that at some conditions the dissociation fraction is not saturated at 100% may be explained by two ways: a/ atomic iodine recombination, which may both decrease the dissociation rate in the discharge and decrease atomic iodine fraction on the passage through injection holes and downstream, b/ converting the discharge energy to ro-vibrationally and electronically excited states of  $I_2$ .

The dissociation limit for the highest  $I_2$  flow rate 0.287 mmol/s was 23%. The dissociation limit coincided roughly with the impedance matching limit; we were not able to match the impedance (decrease the reflected RF power) at power levels 200-250 W, in dependence on the flow conditions.

The fraction of RF power going to dissociation,  $fP_{\text{diss}}$ , (discharge efficiency) is shown in **Fig. 34**.

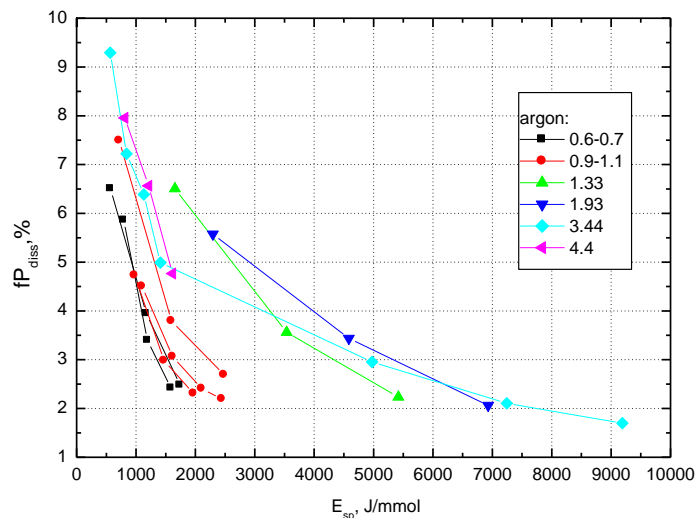


**Fig.34.** Fraction of RF power going to dissociation in dependence on the specific input energy for different Ar flow rates

This figure predicts the best Ar flow rate of about 2 mmol/s; the dependence on the Ar flow rate must be, however, measured more independently on the evaporated  $I_2$  flow, which is the subject for future experiments.

The temperatures averaged across the cavity height were in the range of 275-375 K in subsonic regime. It was found that the average temperature increased significantly with absorbed power only in case when also the dissociation fraction increased with power.

The highest production of atomic iodine was 0.17 mmol/s produced from 0.175 mmol/s of  $I_2$  at the absorbed RF power of 198 W. The dissociation fraction was 49.3% and the discharge efficiency 6.4% in this case.

Comparison of results obtained with  $I_2$  and  $CF_3I$  measured with the same injector (with oval holes) and electrode (95 mm long) are now presented. While the generation of 0.17 mmol/s of atomic iodine required only 11.9 eV/atom in case of  $I_2$ , the similar production of 0.19 mmol/s from  $CF_3I$  required energy nearly twice higher (22.7 eV/atom).

Comparison of the achieved dissociation fraction and discharge efficiency of these two donors in dependence on the specific energy is shown in **Figs. 35, 36**.

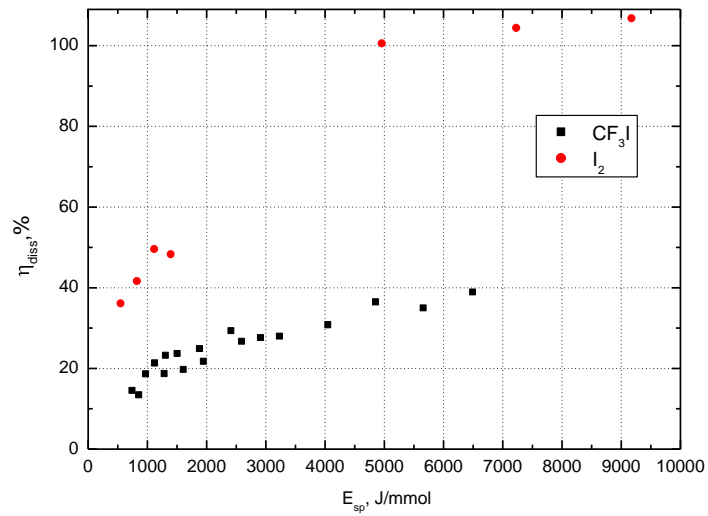


**Fig. 35.** Dissociation fraction of  $\text{CF}_3\text{I}$  and  $\text{I}_2$  in dependence on the specific input energy for selected experimental data  
Similar donor flow rates and RF powers compared

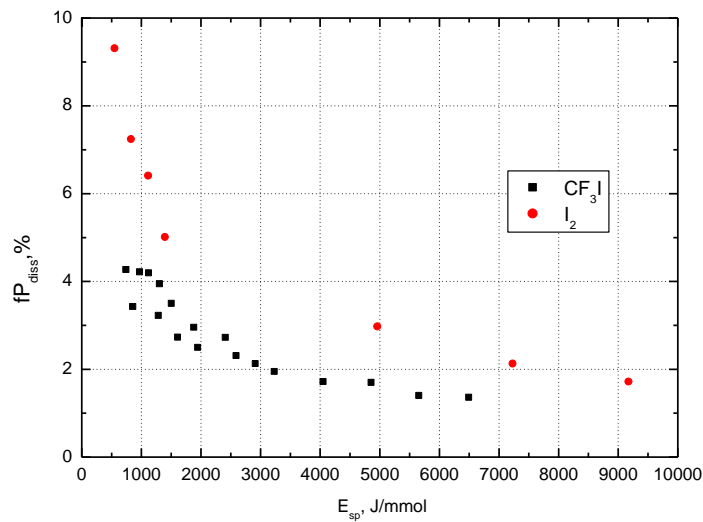


**Fig.36.** Fraction of RF power going to dissociation of  $\text{CF}_3\text{I}$  and  $\text{I}_2$  in dependence on the specific input energy for selected experimental data  
Similar donor flow rates and RF powers compared

It is obvious that molecular iodine is better in both parameters than  $\text{CF}_3\text{I}$ .

#### 6.4. Comparison of four iodine donors studied in DAIG

During the grants on DAIG investigation, four iodine donors' dissociation was studied in the RF discharge, CH<sub>3</sub>I, CF<sub>3</sub>I, HI and I<sub>2</sub>, respectively. Although quite similar maximum atomic iodine production rate 0.15-0.19 mmol/s was achieved from all 4 donors, the efficiency differed between the carbon-contained iodides, HI and I<sub>2</sub>, where the efficiency was increased in this respect. Our experience showed that this efficiency is given predominantly by the kinetic reasons, where the cross-section of dissociative electron attachment and volume back-recombination of the dissociated molecule play the major roles. With the perspective of using this method of atomic iodine generation for a COIL or DOIL operation, the kinetic behavior of the radicals R = CH<sub>3</sub>, CF<sub>3</sub>, H, must be also considered. The important chemical reactions are summarized in **Table 3**. The formation of the compound RO<sub>2</sub> is very fast in the case of all three iodides. This compound is a very serious quencher of both excited iodine and singlet oxygen. Although appropriate rate constants were only derived indirectly and only for R = C<sub>2</sub>H<sub>5</sub>, the authors of [26] suppose similar rates with CF<sub>3</sub> and CH<sub>3</sub> as well.

**Tab. 3**  
Important reactions associated with atomic iodine donors

Reaction	Rate constant	Reference
CH <sub>3</sub> + I → CH <sub>3</sub> I	$9.96 \times 10^{-12} \text{ cm}^3 \text{ s}^{-1}$	18
CF <sub>3</sub> + I → CF <sub>3</sub> I	$3.01 \times 10^{-11} \text{ cm}^3 \text{ s}^{-1}$	19
H + I → HI	not found	
2 I + I <sub>2</sub> → 2I <sub>2</sub>	$3.9 \times 10^{-30} \text{ cm}^6 \text{ s}^{-2}$ $k.[I_2] = 9.4 \times 10^{-13} \text{ cm}^3 \text{ s}^{-1}$ at pI <sub>2</sub> = 1 kPa	20
2 I + Ar → I <sub>2</sub> + Ar	$2.2 \times 10^{-32} \text{ cm}^6 \text{ s}^{-2}$	21
2 I + N <sub>2</sub> → I <sub>2</sub> + N <sub>2</sub>	$1.2 \times 10^{-32} \text{ cm}^6 \text{ s}^{-2}$	22
2 I + wall → I <sub>2</sub>	$\gamma = 1$	estimated
CH <sub>3</sub> + O <sub>2</sub> + Ar → CH <sub>3</sub> O <sub>2</sub>	$1 \times 10^{-30} \text{ cm}^6 \text{ s}^{-2}$	23
CF <sub>3</sub> + O <sub>2</sub> → CF <sub>3</sub> O <sub>2</sub> (in argon)	$1 \times 10^{-11} \text{ cm}^3 \text{ s}^{-1}$	24
H + O <sub>2</sub> → HO <sub>2</sub> (in argon)	$9.47 \times 10^{-11} \text{ cm}^3 \text{ s}^{-1}$	25
I* + RO <sub>2</sub> → I + RO <sub>2</sub> (R = C <sub>2</sub> H <sub>5</sub> !)	$9.47 \times 10^{-11} \text{ cm}^3 \text{ s}^{-1}$	26
O <sub>2</sub> (a) + RO <sub>2</sub> → I + O <sub>2</sub> (x) (R = C <sub>2</sub> H <sub>5</sub> !)	$1.0 \times 10^{-10} \text{ cm}^{-3} \text{ s}^{-1}$	26
O <sub>2</sub> (a) + HO <sub>2</sub> → HO <sub>2</sub> * + O <sub>2</sub> (x)	$3.3 \times 10^{-11} \text{ cm}^{-3} \text{ s}^{-1}$	27

The chemical heat associated with an unavoidable dimerization R + R → R<sub>2</sub> mentioned in Section 6.1.4 is another complication for the laser action in the oxygen-iodine lasers. The advantage of I<sub>2</sub> is, besides the higher dissociation efficiency, an absence of complicating kinetics and the yield of two

iodine atoms per one molecule. Also, even partial predissociation of I<sub>2</sub> could lead to a significant save of the O<sub>2</sub>(<sup>1</sup>Δ) energy, thanks to a positive influence of initial atomic iodine in the system on the complex I<sub>2</sub>- O<sub>2</sub>(<sup>1</sup>Δ) dissociation kinetics. Vibrationally excited molecular iodine, which is most probably produced in the discharge can also have a positive effect on the I<sub>2</sub> dissociation by O<sub>2</sub>(<sup>1</sup>Δ).

On the basis of our research results on the DAIG gained by now, both experimentally and for the kinetic reasons, **molecular iodine seems to be the most promising atomic iodine donor for this generation method.**

## 7. Conclusions

- New experimental results on atomic iodine generation from CH<sub>3</sub>I and CF<sub>3</sub>I were obtained in the CW and pulse-periodic RF discharge mode. Mapping of the atomic iodine concentration, [I], in the vertical cross section of the cavity was performed in both subsonic and supersonic flow conditions. In the supersonic regime, a maximum [I] in the cavity center was  $4.22 \times 10^{14} \text{ cm}^{-3}$ , and a corresponding minimum gas temperature evaluated from the probe measuring was 230 K.
- The [I] mapping along the injector axis indicated a growing generation of iodine atoms along the injector holes from the inlet of RI+Ar mixture. This was confirmed also by modeling results.
- Several hardware changes of the DAIG device, a usage of small traces of NO gas together with a pulse-periodic RF source mode led to a significant improvement of the discharge stability. Thanks to these improvements, nearly highest possible RF power (~500 W) could be loaded into the discharge. The dissociation fraction of CH<sub>3</sub>I then increased from ~16% to 23% and a produced flow rate of atomic iodine to  $0.15 \text{ mmol s}^{-1}$ .
- A usage of the newly fabricated injector with the oval holes resulted in decrease in the discharge pressure by 20% and improvement of the CF<sub>3</sub>I dissociation, so that  $0.19 \text{ mmol s}^{-1}$  of iodine atoms was produced from  $0.9 \text{ mmol/s}$  of CF<sub>3</sub>I at the dissociation fraction of 20.6%.
- Iodine donor HI was newly studied as the atomic iodine source. The results gathered up to now showed that with this donor a better efficiency of the absorbed RF power can be achieved than with CH<sub>3</sub>I/CF<sub>3</sub>I (15% against 10%), and it provided  $0.19 \text{ mmol s}^{-1}$  of produced atomic iodine at 16% dissociation fraction.
- The numerical modeling helped to interpret some experimental features of the process of iodine generation in the RF discharge and to suggest further improvements of experimental conditions

and configurations. By modeling, the elevated temperature measured in the cavity was explained by exothermic recombination of alkyl radicals, forming  $R_2$  molecules. Further, a high rate of I wall recombination was calculated and the results indicated that the dissociation fraction in the discharge may be much higher than measured values in the supersonic cavity tens millimeters downstream from the injector outlet.

- A new solid  $I_2$  evaporator with the heat exchanger was designed, manufactured and used. It is capable to provide very stable iodine vapor flow rate up to 0.3 mmol/s at the evaporator temperature up to 85 °C.
- Molecular iodine was newly studied as the atomic iodine source. Both the dissociation fraction and discharge efficiency were much better than with three iodides at the same input specific energy. A comparable production of atomic iodine as with the iodides was achieved, 0.17 mmol/s, but at much lower donor flow rate, 0.175 mmol  $I_2$ /s and at lower absorbed RF power of 198 W. The dissociation fraction was in the range 20-100% in dependence on the  $I_2$  and Ar flow rates.
- On the basis of the experimental and theoretical studies performed by now,  $I_2$  was selected as the most promising donor for the future gain/laser experiments on COIL or DOIL.

#### **Plans for the next work:**

- Optimization of conditions in experiments with  $I_2$  used as the atomic iodine donor in the DAIG device;
- Testing the DAIG operation with the primary flow containing  $O_2(^1\Delta)$  by joining it to either chemical or discharge SOG; small signal gain measurements, i.e. to fulfill the task of this grant proposal;
- Detection of emission spectra of the RF discharge and afterglow using a newly purchased instrument with sensitive spectrograph and EMCCD camera.

## **8. References**

- [1] Final Report of the Grant No. FA8655-06-1-3034, *Discharge generation of atomic iodine for a COIL*, (PI J. Kodymová), submitted 15 May 2008
- [2] J. Schmiedberger, V. Jirásek, J. Kodymová, K. Rohlena, *Advanced Concept of Discharge Oxygen-Iodine Laser*, 38<sup>th</sup> AIAA Plasmadynamics and Lasers Conference, Miami, FL, USA, June 2007, AIAA Paper 2007-4239, CD Proceedings
- [3] J. Kodymová, O. Špalek, V. Jirásek, M. Čenský, J. Hrubý, J. Schmiedberger, *Contribution to development of chemical and discharge oxygen-iodine lasers*” (Inv. talk), Int. Conference on Lasers, Applications, and Technologies, ICONO/LAT 2007, Minsk, Belarus, May 2007, Proc. SPIE Vol. **6735**, 10-17 (2007)

- [4] V. Jirásek, J. Schmiedberger, M. Čenský, I. Picková, J. Kodymová, O. Špalek, *Plasmachemical generation of atomic iodine for iodine lasers pumped by singlet oxygen*, Chem. Listy **102**, 1327-1331 (2008)
- [5] J. Schmiedberger, V. Jirásek, M. Čenský, J. Kodymová, I. Picková, O. Špalek, *RF discharge generation of I atoms in CH<sub>3</sub>I and CF<sub>3</sub>I for COIL/DOIL*, 17<sup>th</sup> Int. Symposium on gas Flow and Chemical Lasers & High Power Lasers, Sept 2008, Lisbon, Portugal  
Proc. SPIE Vol. **7131**, 71310E-1-8 (2008)
- [6] J. Schmiedberger, V. Jirásek, J. Kodymová, K. Rohlena, *Novel concept of electric discharge oxygen-iodine laser*, European Physical Journal D, Atomic, Molecular, Optical and Plasma Physics **54**, 239-248 (2009)
- [7] Report 001 of the Grant No. FA8655-09-1-3092, *Discharge atomic iodine generator (DAIG) for a COIL*, (PI J. Kodymová), submitted 22 January 2010
- [8] D. L. Baulch, C. J. Cobos, R. A. Cox, P. Frank, G. Hayman, Th. Just, J. A. Kerr, T. Murrells, M. J. Pilling, J. Troe, R. W. Walker, J. Warnatz, *Evaluated kinetic data for combustion modelling. Supplement I*, J. Phys. Chem. Ref. Data **23**, 847-1033 (1994)
- [9] T. F. Hunter, S. Kristjansson, *Optoacoustic method of measuring reaction rates of the radicals CH<sub>3</sub>, CD<sub>3</sub>, C<sub>2</sub>H<sub>5</sub> and CH<sub>2</sub>I with I and I<sub>2</sub>*, J. Chem. Soc. Faraday Trans. 2, **78**, 2067-2076 (1982)
- [10] G. Burns, R. J. LeRoy, D. J. Morris, J. A. Blake, *Recombination of iodine atoms in dilute solutions of argon*, Proc. R. Soc. London A **315**, 81-99 (1970)
- [11] H. W. Changand, G., Burns, *Recombination of iodine atoms by flash photolysis over a wide temperature range. VII. Recombination between 206 and 300°K*, J. Chem. Phys. **64**, 349-353 (1976)
- [12] J. K. K. Ip, G. Burns, *Recombination of iodine atoms by flash photolysis over a wide temperature range. II. I<sub>2</sub> in He, Ar, Xe, N<sub>2</sub>, CO*, J. Chem. Phys. **56**, 3155-3162 (1972)
- [13] G. P. Kota, J. W. Coburn, D. B. Graves, *Heterogeneous recombination of atomic bromine and fluorine*, J. Vacuum Sci. & Technol. A – Vacuum Surfaces and Films **17** (No1) 282-290 (1999)
- [14] T. J. Madden, G. C. Manke II, G. D. Hager, *1-D and 3-D modeling of the all gas-phase iodine laser (AGIL)*, 34<sup>th</sup> AIAA Plasmadynamics and Lasers Conference, Orlando, FL, June 2003, AIAA Paper 2003-4310
- [15] W. Masuda, M. Hishida, N. Azami, *Effects of wall catalysis on the reaction zone structure of a supersonic flow chemical oxygen-iodine laser*, JSME International Journal B **41** (No. 3) (1998)
- [16] M.A. Lieberman and S. Ashida, *Global models of pulse-power-modulated high-density, low-pressure discharges,* Plasma Sources Sci. Technol. **5**, 145 (1996)
- [17] A. P. Napartovich, I. V. Kochetov, N. P. Vagin, N. N. Yuryshev, *Modelling COIL with iodine atoms produced by pulsed electric discharge*, Proc. SPIE, Vol. **6346**, 634637 (2007)
- [18] T. F. Hunter and K. S. Kristjansson, *Optoacoustic method of measuring reaction rates of the radicals CH<sub>3</sub>, CD<sub>3</sub>, C<sub>2</sub>H<sub>5</sub> and CH<sub>2</sub>I with I and I<sub>2</sub>*, J. Chem. Soc. Faraday Trans. 2, vol. 78, 2067 – 2076 (1982)
- [19] G.A. Skorobogatov, O.N. Slesar, N.D. Torbin, *Vestn. Leningr. Univ. Ser. 4: Fiz. Khim.*, Vol **1**, 30 – 37 (1988)
- [20] G. Burns, R. J. LeRoy, D. J. Morris, J. A. Blake, *Recombination of iodine atoms in dilute solutions of argon*, Proc. R. Soc. London A **315**, 81-99 (1970)
- [21] H. W. Changand, G., Burns, *Recombination of iodine atoms by flash photolysis over a wide temperature range. VII. Recombination between 206 and 300°K*, J. Chem. Phys. **64**, 349-353 (1976)
- [22] J. K. K. Ip, G. Burns, *Recombination of iodine atoms by flash photolysis over a wide temperature range. II. I<sub>2</sub> in He, Ar, Xe, N<sub>2</sub>, CO*, J. Chem. Phys. **56**, 3155-3162 (1972)
- [23] D.L. Baulch, C.J. Cobos, R.A. Cox, C. Esser, P. Frank, Th. Just, J.A. Kerr, M.J. Pilling, J. Troe, R.W. Walker, J. Warnatz, *Evaluated kinetic data for combustion modeling*, J. Phys. Chem. Ref. Data **21**, 411 – 429 (1992)
- [24] R. Cooper, J.B. Cumming, S. Gordon, W.A. Mulac, *The reactions of the halomethyl radicals CCl<sub>3</sub> and CF<sub>3</sub> with oxygen*, Radiat. Phys. Chem. **16** (1980)

- [25] J. Hahn, L. Krasnoperov, K. Luther, J. Troe, *Pressure dependence of the reaction  $H+O_2 (+Ar) \rightarrow HO_2 (+Ar)$  in the range 1-900 bar and 300-700 K*, Phys. Chem. Chem. Phys. **6**, 1997 - 1999 (2004)
- [26] T. L. Andreeva, S.V. Kuznetsova , A. I. Maslov, V.N. Sorokin , *Flash photolysis of iodides in the presence of quenching gases. IV. Photolysis of a  $C_2F_5I - O_2$  mixture*, Journal of Quantum Electronics **27**, 497 (1997)
- [27] J. R. Podolske and H. S. Johnston, J. Phys. Chem. **87**, 628-634, 1983

## Acknowledgements

The investigators are very grateful to the US AFRL/DED at Kirtland AFB, NM for the financial support of this research via the USAF EOARD Grant.

We wish to thank Dr. Timothy Madden at the US AFRL/DED for beneficial discussions on the grant tasks and encouragement.

We thank Dr. A. Gavrielides, Program Manager Lasers and Electro-Optics, Mrs. Susan Fuller, Contract Officer, and Mrs. Jeannette Cyrus, Program Analyst at the USAF EAORD for their helpful assistance with the grant processing.